

35976



National Library  
of Canada

Bibliothèque nationale  
du Canada

CANADIAN THESES  
ON MICROFICHE

THÈSES CANADIENNES  
SUR MICROFICHE

NAME OF AUTHOR/NOM DE L'AUTEUR Alan George Seamster

TITLE OF THESIS/TITRE DE LA THÈSE Energy Stragglings of Heavy Charged Particles  
and the Development of a Particle Identification  
Algorithm

UNIVERSITY/UNIVERSITÉ Simon Fraser University

DEGREE FOR WHICH THESIS WAS PRESENTED/  
GRADE POUR LEQUEL CETTE THÈSE FUT PRÉSENTÉE M.Sc.

YEAR THIS DEGREE CONFERRED/ANNÉE D'OBTENTION DE CE GRADE 1976

NAME OF SUPERVISOR/NOM DU DIRECTEUR DE THÈSE Dr. Ralph G. Korteling

Permission is hereby granted to the NATIONAL LIBRARY OF CANADA to microfilm this thesis and to lend or sell copies of the film.

*L'autorisation est, par la présente, accordée à la BIBLIOTHÈQUE NATIONALE DU CANADA de microfilmer cette thèse et de prêter ou de vendre des exemplaires du film.*

The author reserves other publication rights, and neither the thesis nor extensive extracts from it may be printed or otherwise reproduced without the author's written permission.

*L'auteur se réserve les autres droits de publication; ni la thèse ni de longs extraits de celle-ci ne doivent être imprimés ou autrement reproduits sans l'autorisation écrite de l'auteur.*

DATED/DATE November 22, 1976 SIGNED/SIGNÉ

PERMANENT ADDRESS/RÉSIDENCE FIXÉE

[Redacted address information]



National Library of Canada

Cataloguing Branch  
Canadian Theses Division

Ottawa, Canada  
K1A 0N4

Bibliothèque nationale du Canada

Direction du catalogage  
Division des thèses canadiennes

## NOTICE

The quality of this microfiche is heavily dependent upon the quality of the original thesis submitted for microfilming. Every effort has been made to ensure the highest quality of reproduction possible.

If pages are missing, contact the university which granted the degree.

Some pages may have indistinct print especially if the original pages were typed with a poor typewriter ribbon or if the university sent us a poor photocopy.

Previously copyrighted materials (journal articles, published tests, etc.) are not filmed.

Reproduction in full or in part of this film is governed by the Canadian Copyright Act, R.S.C. 1970, c. C-30. Please read the authorization forms which accompany this thesis.

**THIS DISSERTATION  
HAS BEEN MICROFILMED  
EXACTLY AS RECEIVED**

## AVIS

La qualité de cette microfiche dépend grandement de la qualité de la thèse soumise au microfilmage. Nous avons tout fait pour assurer une qualité supérieure de reproduction.

S'il manque des pages, veuillez communiquer avec l'université qui a conféré le grade.

La qualité d'impression de certaines pages peut laisser à désirer, surtout si les pages originales ont été dactylographiées à l'aide d'un ruban usé ou si l'université nous a fait parvenir une photocopie de mauvaise qualité.

Les documents qui font déjà l'objet d'un droit d'auteur (articles de revue, examens publiés, etc.) ne sont pas microfilmés.

La reproduction, même partielle, de ce microfilm est soumise à la Loi canadienne sur le droit d'auteur, SRC 1970, c. C-30. Veuillez prendre connaissance des formules d'autorisation qui accompagnent cette thèse.

**LA THÈSE A ÉTÉ  
MICROFILMÉE TELLE QUE  
NOUS L'AVONS REÇUE**

ENERGY STRAGGLING OF HEAVY  
CHARGED PARTICLES AND THE  
DEVELOPMENT OF A PARTICLE  
IDENTIFICATION ALGORITHM

by

ALAN GEORGE SEAMSTER

B.Sc., Washington State University, 1974

A THESIS SUBMITTED IN PARTIAL FULFILLMENT OF  
THE REQUIREMENTS FOR THE DEGREE OF  
MASTER OF SCIENCE  
in the Department  
of  
Chemistry

© ALAN GEORGE SEAMSTER 1976

SIMON FRASER UNIVERSITY

October 1976

All rights reserved. This thesis may not be  
reproduced in whole or in part, by photocopy  
or other means, without permission of the author.

APPROVAL

Name: Alan George Seamster

Degree: Master of Science

Title of Thesis: Energy Straggling of Heavy Charged  
Particles and the Development of a  
Particle Identification Algorithm

Examining Committee:

Chairman: Dr. F.W.B. Einstein

-----  
Dr. R.G. Korteling  
Senior Supervisor

-----  
Dr. E.J. Wells

-----  
I.M. Thorson

-----  
Dr. C.H.W. Jones  
External Examiner  
Associate Professor  
Department of Chemistry  
Simon Fraser University

Date Approved: October 27, 1976

PARTIAL COPYRIGHT LICENSE

I hereby grant to Simon Fraser University the right to lend my thesis or dissertation (the title of which is shown below) to users of the Simon Fraser University Library, and to make partial or single copies only for such users or in response to a request from the library of any other university, or other educational institution, on its own behalf or for one of its users. I further agree that permission for multiple copying of this thesis for scholarly purposes may be granted by me or the Dean of Graduate Studies. It is understood that copying or publication of this thesis for financial gain shall not be allowed without my written permission.

Title of Thesis/Dissertation:

Energy Straggling of Heavy Charged Particles  
and the Development of a Particle Identification  
Algorithm

Author:

(signature)

Alan George Seamster

(name)

November 24, 1976

(date)

## ABSTRACT

Energy straggling for protons of 2.0 to 14.0 MeV/amu and for alpha particles of 2.0 to 7.5 MeV/amu is measured in various silicon surface barrier DE detectors. The straggling widths are found to decrease with increasing particle energy, as expected. The measured widths are then compared to the theoretical predictions of Tschalar. In general, the calculated values agree within statistics, with some anomalies. Comparisons of the percent resolution, given by  $\text{FWHM/DE} \%$ , with the percent energy dropped in the DE detector are made. Minima in the resolutions are found beyond percent energy losses of 20% for protons incident on a 76.0 micron detector and beyond losses of 15% for alpha particles incident on a 33.8 micron detector.

A new particle identifying algorithm is developed, based on the Bethe-Bloch equation. Both inner shell electron and charge pick-up corrections are included. This algorithm is valid at non-relativistic energies for protons through fluorine. When combined with a telescope utilizing a 16.6 micron DE detector, mass resolution is observed through Be, with elemental separation through fluorine.

iv

To Jean

V

ACKNOWLEDGMENTS

I want to express my gratitude to Dr. Ralph G. Korteling for his supervision and assistance. I also want to thank Dr. Ray E. Green for the many hours of instruction and explanations.

My sincere appreciation goes to Roger Toren and Wimm Wieseahn for their consultation and programming.

## TABLE OF CONTENTS

	Page
ACKNOWLEDGEMENTS.....	v
LIST OF TABLES.....	viii
LIST OF FIGURES.....	ix
1.0: INTRODUCTION.....	1
2.0: ENERGY LOSS THEORY.....	5
2.1: Interaction of Heavy Charged Particles with Matter.....	5
2.2: Energy Straggling of Heavy Charged Particles.....	11
3.0: CHARGED PARTICLE IDENTIFICATION.....	19
3.1: Silicon Surface Barrier Detectors.....	19
3.2: Detector Telescopes.....	26
3.3: Particle Identification Methods.....	34
4.0: EXPERIMENTAL PROCEDURES.....	46
4.1: Physical Configuration.....	46
4.2: Electronics.....	49
4.3: Calibration.....	52
4.4: Data Acquisition System.....	53
4.5: Off-line Data Analysis.....	54
5.0: RESULTS OF STRAGGLING MEASUREMENTS.....	56
5.1: Proton Straggling.....	57
5.2: Alpha Particle Straggling.....	60
5.3: Theoretical Problems.....	63
5.4: Optimization of the DE-E Technique.....	66

## TABLE OF CONTENTS

	Page
6.0: ALGORITHM DEVELOPMENT.....	71
CONCLUSION.....	93
APPENDIX A.....	96
APPENDIX B.....	99
LIST OF REFERENCES.....	104

## LIST OF TABLES

Table		Page
I	Physical properties of silicon.....	25
II	Telescope configurations.....	48
III	Values of $A_i Z_o^2$ calculated with the final algorithm.....	92

ix  
LIST OF FIGURES

Figure		Page
1	Energy loss distributions for $K = 1.0$ to $K = 0.01$ , $\phi$ is the probability of a particular energy loss.....	16
2	Schematic diagram of a totally depleted silicon surface barrier detector.....	21
3	Detector stack orientation.....	31
4	Gas DE telescope.....	33
5	The effect of including the arbitrary $E_0$ correction in the multiplier algorithm...	37
6	Plot of $MZ^2$ for ions of $Z < 10$ , known to be stable against particle break-up.....	42
7	Electronics for a five detector system,...	50
8	Proton straggling in a 76 micron Si detector.....	58
9	Proton straggling in a 476 micron Si detector.....	59
10	Alpha particle straggling in a 12.9 micron Si detector.....	61
11	Alpha particle straggling in a 33.8 micron Si detector.....	62
12	Percent resolution of protons in a 76 micron Si detector.....	68
13	Percent resolution of alpha particles in a 33.8 micron Si detector.....	70

x  
LIST OF FIGURES

Figure		Page
14	PI spectrum using the uncorrected algorithm as presented in equation 30.....	76
15	Contour plot of ET verses PI using the uncorrected algorithm as presented in equation 30.....	77
16	The K-shell stopping number correction is plotted against the reciprocal of the K-shell quantum number. $O_k$ for Si = .724 .....	79
17	PI spectrum using the algorithm with the $C_k$ correction as presented in equation 36 .....	81
18	Contour plot of ET verses PI using the algorithm with the $C_k$ correction as presented in equation 36.....	82
19	The effective charge of heavy ions as a function of the particle charge and energy .....	84
20	Contour plot of ET verses PI using the algorithm with both the $C_k$ and charge pick-up corrections as presented in equation 40.....	87

## LIST OF FIGURES

Figure		Page
21	PI spectrum using the algorithm with both the $C_k$ and charge pick-up corrections as presented in equation 40.....	88
22	Raw DE data and related PI values for the lithium region.....	91

1.0: INTRODUCTION

The increasing use of DE-E detector telescopes for the identification of heavy ions has brought renewed interest to the study of the energy loss processes of heavy charged particles in matter. Of these processes, those that affect the resolution of a detector telescope are of primary interest to this study. Energy straggling of charged particles is one of the more important concerns, as discussed by Bichsel (1).

Our interest in the area arrives from the need to identify the fragments emitted from Ag as a result of nuclear reactions induced by 200-500 MeV protons. In this major experimental program, the mechanisms of fragment emission are being studied. This requires optimum particle resolution in order to discern the effects as a function of fragment mass and atomic number. These fragments are identified by the DE-E telescope technique and there are some restrictions to the available particle resolution. In order to improve the particle resolving power, it is necessary to study in detail the energy-loss processes of heavy charged particles in the silicon surface barrier detectors used

in this experiment. This information combined with an improved particle identification algorithm will enhance the identification of the emitted fragments and will set limits on the technique.

Energy straggling in the DE detector, in particular, can substantially limit the isotopic resolution of a detector telescope. Despite its importance, very few measurements have been made concerning silicon surface barrier detectors. Information of this type would aid the experimentalist in choosing a telescopic configuration that would offer the optimum resolution of the particles and energies of interest. Furthermore, these measurements would allow the applicability of current straggling theories to be tested.

Aside from the measurements of physical processes, one can approach the optimum resolution of a detector telescope by developing a particle identifying algorithm which is sensitive to the changing conditions surrounding the energy loss of a charged particle as it travels through an absorber. Many algorithms are available to the experimentalist, however very few are valid over a wide range of

particles and energies. The current expressions, which sufficiently cover the particles and energies of interest, are generally based on empirical relations and disregard theoretical considerations.

The development of an algorithm from theoretical principles should facilitate the incorporation of those expressions which are sensitive to the changing charge and velocity of heavy ions as they pass through an absorber.

To provide a better understanding of the physical processes which govern the measurements used in this study, we will begin with a brief discussion of the theoretical background of the interaction and energy straggling of charged particles in matter. With this preparation we will continue with a discussion of the state-of-the-art of silicon surface barrier detectors and their use in detector telescopes.

As the major scope of this study is aimed towards the improvement of the particle resolution of the DE-E technique, it is necessary to review those particle identification methods used in relation with this technique. This discussion will also demonstrate

some of the limitations involved with particle analysis. Following this section, we will present the experimental procedures utilized in this study. This will include a description of the detector telescopes and the associated electronics. The data acquisition system and the off-line analysis will be discussed as well. The results of the straggling measurements will be presented next, with regard to the theoretical predictions of Tschalar. This data will also be used to indicate in which energy loss regions, optimum energy resolution may be obtained.

Following the straggling data discussion, we will conclude with the derivation of a particle identification algorithm based on the Bethe-Bloch relation. Unlike most algorithms, this one includes corrections for atomic binding as well as charge pick-up. Examples of particle spectra obtained with this algorithm will be presented at this time.

## 2.0: ENERGY LOSS THEORY

### 2.1: Interaction of Heavy Charged Particles with Matter

As discussed by Uehling (2), high energy heavy particles are in a stripped or highly charged state after entering an absorber. The inelastic collisions with the absorber's atomic electrons are the major mode of energy loss at this early stage. These interactions often transfer sufficient energy to eject the electrons involved, resulting in ionization. Nuclear collisions, which involve the recoil of the atoms in the substance, are relatively rare at these higher velocities and do not contribute significantly to the energy loss. At velocities greater than the velocity of the K-shell electrons of the incident ion, the charged particle will have a small probability of capturing an electron from the medium, however any captured electron will be lost in the following collision. The probability of electron capture reaches a maximum when the velocity of the ion equals the velocity of its own inner shell electrons. At this point, the nuclear collision probability has increased and these interactions will become more predominant as the ion continues to slow down. As velocities are reached comparable to less

tightly bound electrons, electron capture continues, until a neutral atom is produced. The rate of energy loss of the particle changes continuously during its journey. As we shall see this fact, along with other features, contributes to the difficulty of theoretically solving the energy loss problem.

The first modern relations concerning the energy loss of a given particle through a particular material were expressed by Bohr (3),(4). He gave the energy loss as:

$$\frac{dE}{dx} = \frac{-4\pi e^4 Z_i N Z}{m_0 V^2} \int_0^{\infty} \frac{b db}{b^2} \quad 1.$$

where:  $e$  = electron charge  
 $N$  = atom density of the absorber  
 $Z_i$  = atomic number of the incident particle  
 $Z$  = atomic number of the absorber  
 $m_0$  = electron mass  
 $V$  = particle velocity  
 $b$  = impact parameter of the particle-electron collisions

The integral containing the impact parameter must be taken over the range bound by the maximum and

minimum energy transfer. This allows expression 1 to be restated as:

$$\frac{dE}{dx} = \frac{-2\pi e^4 Z_i N Z}{m_0 V^2} \int_{\min}^{\max} \frac{\epsilon d\epsilon}{\epsilon^2} \quad 2.$$

where  $\epsilon$  is the kinetic energy transferred. Equation 2 may be readily reduced to:

$$\frac{dE}{dx} = \frac{-2\pi e^4 Z_i^2 N Z}{m_0 V^2} \ln \frac{\epsilon_{\max}}{\epsilon_{\min}} \quad 3.$$

A further term was added to correct for the increase in the maximum energy loss and the decrease in the minimum loss produced by the Lorentz contraction of the coulomb field of the heavy particle. this correction leaves us with the final expression:

$$\frac{dE}{dx} = \frac{-2\pi e^4 Z_i^2 N Z}{m_0 V^2} \left[ \ln \frac{\epsilon_{\max}}{\epsilon_{\min}} - \ln(1-\beta^2) - \beta^2 \right] \quad 4.$$

Bethe (5) treated the energy loss problem by applying the Born approximation to the collisions between the charged particle and the atomic electrons. He introduced the average excitation potential of the

atomic electrons,  $I$ , where:

$$I^2 = \epsilon_{\max} \cdot \epsilon_{\min}$$

The Bohr term,  $\ln \epsilon_{\max} / \epsilon_{\min}$ , could then be expressed as:

$$\ln \frac{\epsilon_{\max}}{\epsilon_{\min}} = 2 \ln \frac{\epsilon_{\max}}{I} \quad 5.$$

Assuming  $\epsilon_{\max}$  results from a head-on collision such that the energy transferred is  $2m_0V_i^2$ , equation 4 may be rewritten as:

$$\frac{dE}{dx} = \frac{-4\pi e^4 Z_i^2 NZ}{m_0V^2} \left[ \ln \frac{(2m_0V^2)}{I} - \ln(1-\beta^2) - \beta^2 \right] \quad 6.$$

This particular expression is referred to as the Bethe-Bloch equation. This form will produce the energy loss, assuming that any loss of energy due to elastic scattering on nuclei or Cerenkov radiation is negligible, for particles with an energy  $> 1.5$  MeV per nucleon passing through light absorbers. When working with lower energy particles, an inner shell correction term,  $(C/Z)$  is inserted:

$$\frac{dE}{dx} = \frac{-4\pi e^4 Z_i^2 NZ}{m_0V^2} \left[ \ln \frac{2m_0V^2}{I(1-\beta^2)} - \beta^2 - \frac{C}{Z} - \frac{\delta}{2} \right] \quad 7.$$

The low energy term  $C/Z$ , as described by Paul (6), arises out of the nonparticipation of the inner shell electrons of the atoms when the velocity of the incident particle is comparable to the electron velocity. The stopping power under these conditions, is considerably reduced. As presented by Whaling (7), the  $C_K$  correction reduces the value of  $dE/dx$  by 4.5% in Be ( $I=57\text{eV}$ ) for protons of 1.0 MeV and by 9% at 0.2 Mev. However, this effect is not very large for an absorber of low atomic number when the velocity of the incident particle is greater than the velocity of the K-shell electrons, where  $V_K=(Z_A/137)C$ . For materials with a high value of  $Z$ , the  $C_K$  correction will be necessary over a broader range of particle energies. However, in those instances where the K-shell electrons represent a small percentage of the total electrons, the magnitude of the correction will be small. The energy loss equation can be corrected by including the  $C/Z$  shell term. Walske (8),(9) derived suitable expressions for both the K and the L-shell terms.

At higher energies,  $\geq 40$  MeV/amu, (10), cooperative effects among the atoms of the medium become important unless the density of the medium is very low. The absorber material is polarized by the

field of the charged particle and when the velocity exceeds a critical value, which is determined by the dielectric properties of the medium, ionization and energy losses are reduced. The magnitude of this correction depends on the dispersive properties of the medium. Sternheimer (10) calculated this correction for a number of materials, including silicon. This correction is given by:

$$\delta = 4.606 X + C + a(X_1 - X)^m \quad 8.$$

with  $X = \log(p/m_0C)$ , where  $p$  and  $m_0$  are the momentum and the rest mass of the incident particle.  $X$ ,  $X_1$ ,  $m$ , and  $a$  are constants which are characteristic of the substance considered.

Several computer programs and tables currently exist for calculating the range or energy loss of several ions in a wide range of absorbers. Those most commonly referred to include the work by Lindhard and Scharff (11), Northcliffe and Schilling (12), Armstrong and Chandler (13), Steward (14), and others. These tables and programs are based on the relations previously presented although combinations and/or further corrections are commonly used. Most of the available calculations agree in the medium and upper energy ranges, however large discrepancies are noted in the low energy range, below 1 MeV per amu.

## 2.2: Straggling of Heavy Charged Particles

The statistical nature of the energy loss process produces fluctuations of energy losses of charged particles as they pass through an absorber. This effect results in a gradual increase in the width of the energy distribution as the particles penetrate the material. Straggling effects are commonly discussed in relation with a few useful terms; the most probable energy loss, which is normally given by the maximum of the energy spectrum measured experimentally; the difference between the most probable energy loss and the average energy loss, where the average energy loss is given by the theoretical expressions; and the resolution or full-width-at-half-maximum of the distribution.

Straggling theory is separated into three major regions. These areas include the region where heavy particles are penetrating thick absorbers causing energy losses which make up a large fraction of the initial energy of the particle; the region consisting of high energy charged particles passing through thin absorbers losing only a small fraction of their incident energy; and of course the area bordered by

these two extremes. Several authors have derived expressions for the straggling expected in each of these areas. We shall discuss those commonly used by the present day experimenters.

Bohr (15) derived relations for the region of large energy losses. He divided the energy distribution into small groups where the energy loss in each group was relatively constant. If the total number of collisions in each group is large, the resultant energy loss distribution will be Gaussian with a variance given by:

$$\sigma^2 = 4\pi e^4 Z_i^2 N Z x \quad 9.$$

while the resolution is given by:

$$\Omega = 2.35 \sigma \quad 10.$$

where:

e = electron charge

$Z_i$  = atomic number of the particle

N = density of atoms in the absorber

x = absorber thickness

At this time, we shall define the following parameter:

$$K = \epsilon / \epsilon_{\max} \quad 11.$$

where:

$$\epsilon = \frac{2 \pi e^4 Z_i^2 N Z x}{m_0 V^2} \quad 12.$$

Bohr's expressions will be valid for the following region:

$$K \gg 1$$

The average energy loss and the most probable energy loss are found to coincide in this area.

Landau (16) studied the opposing situation

where:

$$K \ll 1$$

In this case we are concerned with high energy charged particles traversing thin absorbers. The resultant distribution is asymmetric, with a large width around the most probable energy loss. As very few collisions occur in the high energy subgroup, the most probable energy loss is followed by a long tail. The width of this distribution is given by:

$$\text{FWHM}_{\text{Landau}} = 3.98 \epsilon \quad 13.$$

The most probable energy loss occurs at a lower value than the average energy loss prediction. The following expression gives the most probable energy transfer:

$$\Delta_{\text{mp}} = \epsilon \left\{ \ln \left[ \frac{2 m_0 V^2 \epsilon}{I^2 (1 - \beta^2)} \right] - \beta^2 + .37 \right\} \quad 14.$$

Using the modified Bethe-Bloch relation, the difference between the average and the most probable energy loss produces a measure of the asymmetry of the distribution.

The intermediate region was first solved by Symon (17). His approximations include the fact that the width of the distribution changes not only due to

statistical fluctuations but also because particles with different energies lose energy at different average rates. Unfortunately for large energy losses Symon's expressions predict distributions with a skewness too small by a factor of two or more.

This central region was solved exactly by Vavilov (18). Furthermore his expressions reduce to Bohr and Landau relations at the two extremes. In general the Vavilov functions are valid where:

$$0.01 \leq K \leq 1$$

Figure 1 illustrates the distribution transitions resulting from following  $K = 0$  (Landau region) to  $K = 1.0$ , with a value of  $\beta^2 = 0.9$ . The skewness parameter,  $\lambda$ , is given by:

$$\lambda_v = \frac{dE - d\bar{E}}{\epsilon_{\max}} - (1 + \beta^2 - .577216) \quad 15.$$

which is related to the original Landau asymmetry factor

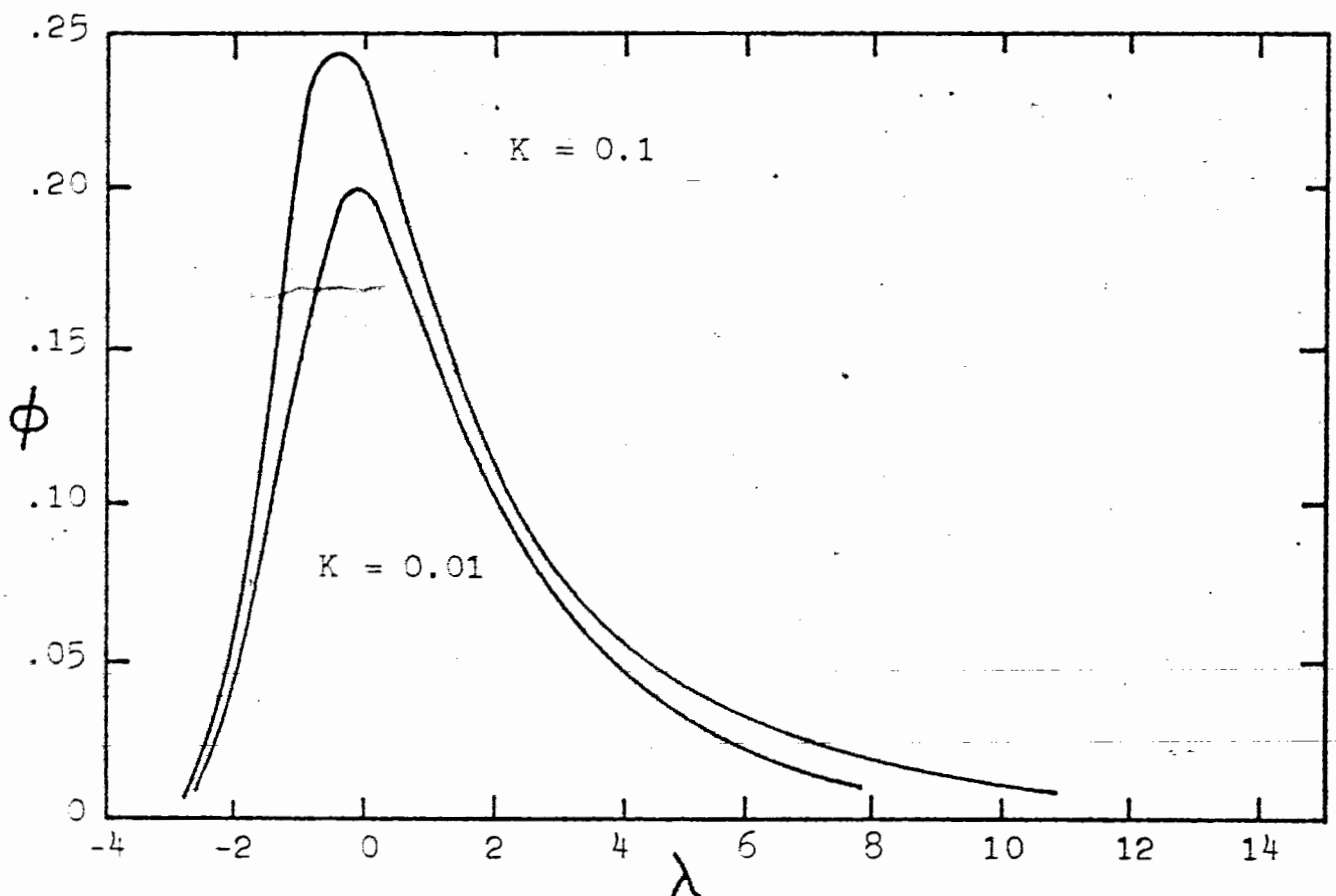
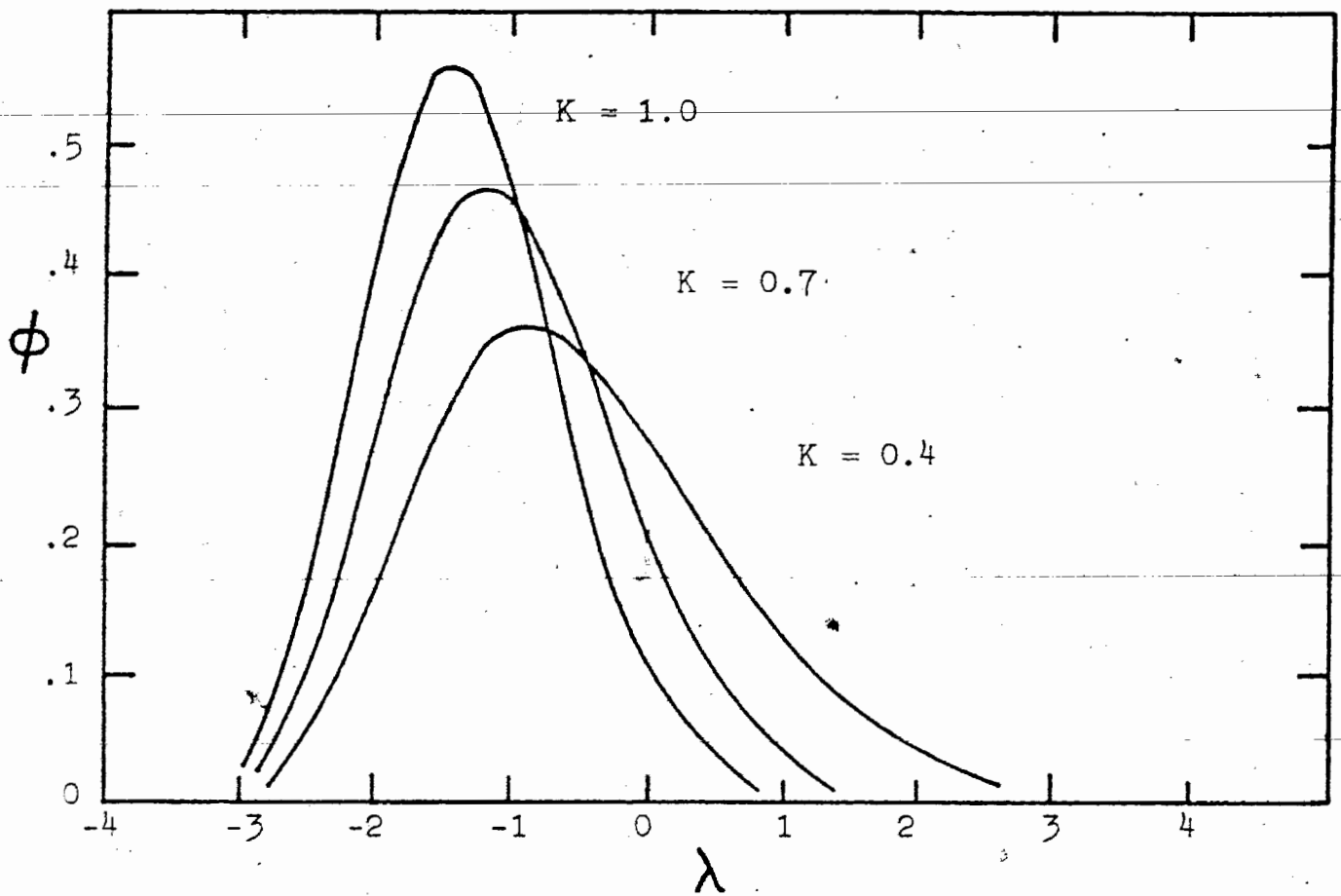


Figure 1. Energy loss distributions for  $K = 1.00$  to  $K = 0.01$ .  $\phi$  is the probability of occurrence of a particular energy loss.

by the following expression:

$$\lambda = \frac{\lambda_v}{K} - \log K \quad 16.$$

For our purposes  $\lambda$  can be taken as being proportional to the difference between the average energy loss and the most probable energy loss. The calculation of the Vavilov distribution is rather involved, however Seltzer and Berger (19) have generated tables of  $K$  verses  $\beta^2$  for the range of values:

$$0.01 \leq K \leq 10.0$$

$$0.00 \leq \beta^2 \leq 1.00$$

along with the related skewness parameters.

Several studies have been published supplying experimental data for conformation of these straggling expressions. The work in the high energy loss region is lead by Tschalar (20,21,22). He has found that very large energy loss distributions deviate somewhat from

that predicted by the Bohr theory. These distributions have a low energy tail, however they are still generally gaussian. Work has also been published by Payne (23) in this same area and his results coincide with Tschalar's. Tschalar's work is explained in more detail in Appendix B.

The most notable work in the thin absorber region has been done by Bishsel (1) and by Maccabee (24,25). Both groups demonstrated excellent agreement with the straggling theory of Vavilov, for low  $Z$  incident ions.

### 3.0: CHARGED PARTICLE IDENTIFICATION

#### 3.1: Silicon Surface Barrier Detectors

Since the identification of charged particles by the telescope technique is based on the interactions of these particles with the detector material, it is instructive to discuss the preparation and use of the detectors employed in these measurements.

Although silicon is not the only material utilized in solid-state transmission detectors; its properties, as outlined in Table I, make it superior in resolution, while still allowing the production of a compact, fairly rugged and stable unit, easily adapted to the detector telescope. Totally depleted detectors of this type have been available commercially for a relatively short time, in a wide range of thicknesses. Their use has contributed markedly to the state-of-the-art of the DE-E telescope technique.

The characteristics and construction of silicon surface barrier detectors are reviewed by Bertolini (26) and Poenaru (27). Totally depleted silicon surface barrier detectors, as used in DE-E telescopes,

are constructed from high purity silicon with impurity levels in the part-per-billion range. The resistivity of the silicon is chosen to give the optimum field strength, (volt/cm) for the best charge collection, at each particular detector thickness necessary for superior resolution.

Figure 2, from the detector manual by Ortec (28), illustrates the basic construction of this type of detector, where  $D$  represents the diameter of the active area and  $W$  is the depth of the depleted region, which can range from 5 microns to 5 millimeters. The active volume of the detector contains an electric field which results from the applied reverse bias. The passage of ionizing radiation creates free charge carriers which are separated by the electric field. By integrating the resultant current a charge proportional to the energy deposited within the active volume of the detector is produced.

The preparation of the original silicon wafer involves exacting mechanical processing and etching of an N-type silicon monocrystal. In order to insure thickness uniformity in the thin DE detector, the crystal is cut with a diamond saw and no more than 20

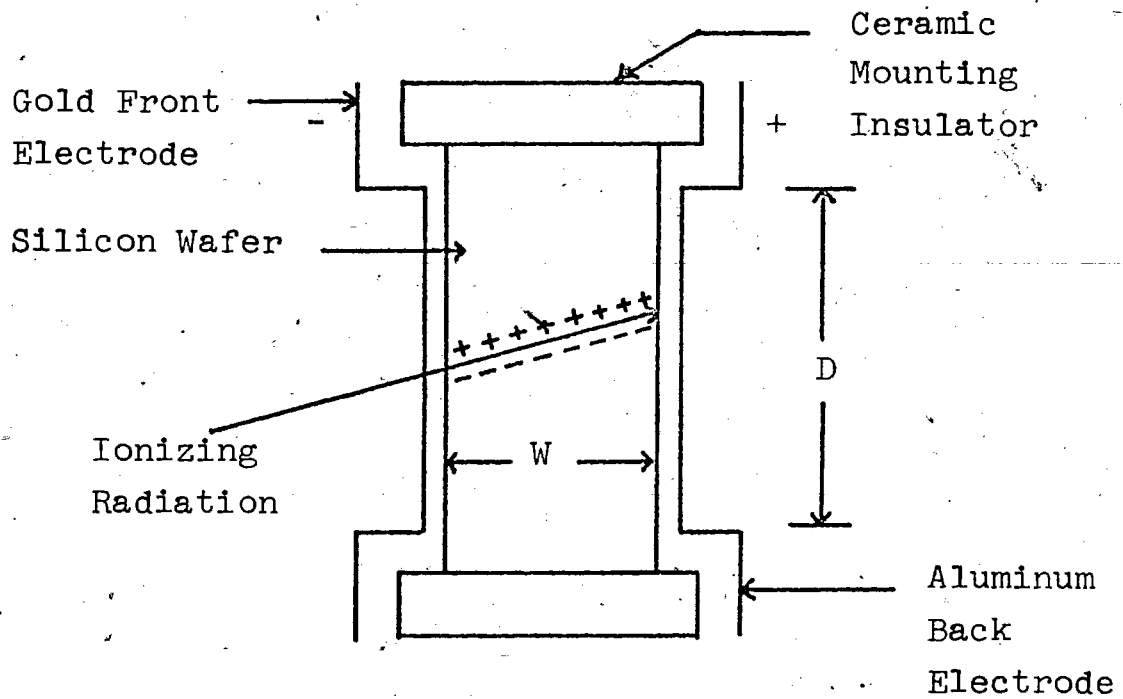


Figure 2. Schematic diagram of a totally depleted silicon surface barrier detector.

microns are removed during etching. The minimum detector thickness is restricted by the increase in capacitance as the thickness decreases. This increase produces a rise in the electronic noise with a magnitude which could be greater than or equal to the actual measured energy losses of charged particles. The contributions of detector and electronic noise, to the observed energy widths, are given by the following expression as presented by Bertolini (26):

$$(\text{FWHM})^2_{\text{obs}} = (\text{FWHM})^2_{\text{strag}} + (\text{FWHM})^2_{\text{det}} + (\text{FWHM})^2_{\text{elec}}$$

After etching, a P-type inversion layer is produced by chemical treatment with oxygen rich substances such as hydrogen peroxide and ozone. The rectifying contact with this inversion layer is made through the gold layer deposited by vacuum evaporation. It is necessary that this layer not be too thick. A transparent film corresponding to 75% light transmission is satisfactory. This allows a thickness range of 20-40  $\mu\text{g}/\text{cm}^2$ , which makes it necessary to run these detectors in total darkness. The rear ohmic contact is aluminum, approximately 40  $\mu\text{g}/\text{cm}^2$  thick.

This surface must be thin to insure a negligible injection of charged carriers.

As discussed by Wang (29), several metals other than gold may be utilized. Some manufacturers use platinum in order to avoid the formation of an amalgam with the mercury vapors coming from the diffusion pumps. It appears, nevertheless, that the resistances of all the possible substitutes become identical after several months, probably as a consequence of a slow oxygen diffusion across the metal. This fact suggests that the rectification process at the contact is more closely related to the porosity of the metal and of the oxide and to its reactivity with oxygen rather than to its work function.

An early problem with the thinner detectors as discussed by Goulding and Harvey (30) involved ion-channeling which resulted in energy losses lower than expected for those ions being channeled. It was observed that heavy ions have a longer range when penetrating the crystal along a principal axis than in the case of penetrating along another direction (27). This phenomenon was explained as ion channeling due to a series of collisions with the lattice atoms. As the

crystal structure is more open along a principal axis, the ions focus the track in a more linear way than in the case of random collisions. This problem is eliminated by cutting the silicon wafers at an angle of 10 to 20 degrees from the plane.

The efficiency of silicon detectors for charged particles is essentially 100% for any case where the energy lost in the sensitive region is much larger than the noise level. This feature, along with their other attributes, make these devices excellent counters for charged particles.

Table I: Physical Properties of Silicon (28)\*

---

Atomic Density	$5.0 \times 10^{22}$ atoms-cm <sup>-3</sup>
Density	2.33 gm-cm <sup>-3</sup>
Dielectric Coefficient	12
Energy Gap	1.1 eV
Energy per Electron-Hole Pair	3.6 eV-pair
Mobility	
Electron	1350 cm <sup>2</sup> -volt <sup>-1</sup> -sec <sup>-1</sup> ( $2.1 \times 10^9$ T <sup>-2.5</sup> cm <sup>2</sup> -volt <sup>-1</sup> -sec <sup>-1</sup> )
Hole	480 cm <sup>2</sup> -volt <sup>-1</sup> -sec <sup>-1</sup> ( $2.3 \times 10^9$ T <sup>-2.7</sup> cm <sup>2</sup> -volt <sup>-1</sup> -sec <sup>-1</sup> )
Thermal Expansion, linear	$4.2 \times 10^{-8}$ (°C) <sup>-1</sup>

\* Quantities correspond to 25 degrees centigrade unless otherwise indicated.

### 3.2: Detector Telescopes

In this section, the following symbols will be referred to repeatedly:

Z ----- atomic number

A ----- mass number

$E_T$  ----- total kinetic energy

M ----- mass in amu

dE ----- energy deposited in a thin solid-state  
transmission detector

dx ----- the thickness of the thin solid-state  
transmission detector

DE ----- the first detector in a telescope

E ----- the second or stopping detector in a telescope

In order to identify a nuclear particle produced in a nuclear reaction, it is necessary to determine its atomic number,  $Z$ , and mass number  $A$ . A successful identification of  $Z$  and  $A$  involves measuring quantities that are related yet independent functions of these values. In the case of non-relativistic particles, with which this study is solely concerned,  $A$  can be described by the mass of the particle in amu,  $M$ . Although  $M$  can be measured by time-of-flight techniques

as described by Butler, Poskanzer, and Landis (32), its absolute value is not necessarily required for the identification of the lighter particles, hydrogen through Be. Mass resolution above this region can be enhanced by increasing the DE detector thickness. However, such an increase is followed by a rise in the low energy cut-off for all particles incident on the telescope. This problem is resolved by utilizing time-of-flight for the mass determinations of these heavier particles. For isotopic resolution of the lighter elements, a measurement of the energy loss of a nuclear particle passing through a thin transmission solid-state detector coupled with the measurement of the residual energy of the particle in a second thicker solid-state detector can be used to indirectly measure the quantity  $MZ^2$ .

$$\frac{dE}{dx} \propto \frac{MZ^2}{E_T} \quad 17.$$

where  $dE$  is the energy deposited in the thin detector of thickness  $dx$  and  $E_T$  is given by the sum of this loss and the measured residual energy. The various methods that are currently available for converting these measured quantities into values relating to  $MZ^2$  will be

described in a separate section.

Detector telescopes and their applications have been reviewed by Goulding and Harvey (30). The basic detector telescope, as described by Goulding, Landis, Cerny, and Pehl (33),(34), consists of two totally depleted silicon surface barrier detectors; a thin dE detector followed by a much thicker E detector separated by a few centimeters. As a nuclear particle passes through the first detector a signal is produced proportional to the energy lost by the particle. In a similar manner, assuming that the E detector is sufficiently thick to stop the particle, the signal in the second detector will be proportional to the residual energy of the particle. Thus, the sum of the two signals will give  $E_T$ .

In an experimental situation, many different particles are traversing through the telescope at the same time. In order to match the proper DE signal with its associated E signal a coincidence circuit is employed. Furthermore, in several instances, particles will be produced with sufficient energies to carry them through both detectors, resulting in an erroneous  $E_T$  determination. This problem is alleviated by adding an

E-reject detector following the E detector. A signal, originating in this detector will act as a veto if it is in coincidence with the signals from the first two detectors. It is very important that the dead layer on the front of the E-reject detector be as small as possible in order that those particles that barely exit the E-detector can get into the active portion of the E-reject detector and create a measurable signal.

In more complex experiments, several thin detectors can be used in the telescope stack, in order to maximize the range of particles observable and resolvable by the system.

In most cases, the stack of detectors is placed in a detector block, which keeps the detectors in line with each other. Collimator rings, machined from 1.0 mm copper, with varying sized inner diameters are placed in front of each detector, except for the E-reject. The inner diameter of the collimator defines the active area of the detector, thus the solid angle for the experiment when combined with the target to DE distance. The detector housing ring could be used as a collimator however non-uniformities in the dead layer exist near the active surface edge. Furthermore,

particles that enter the detector near its edge are apt to miss the active area of the second detector due to its original trajectory. Figure 3 illustrates a standard detector stack orientation.

Therefore, for the identification of light particles,  $A < 6$ , with good energy resolution, silicon surface barrier detector telescopes are generally used as they offer the advantages of a compact and relatively sturdy construction which allows the on-line analysis of high fluxes of nuclear particles. However if one desires to identify low energy heavy particles, it is necessary to use a telescope utilizing a gas DE detector as described by Barrette et al (31). Although they are more difficult to use and maintain, they have distinct advantages over conventional solid-state detectors. Once the unit is constructed, an infinite number of thin DE detectors of varying thicknesses can be produced by changing the gas pressure as well as the type of gas used. The homogeneity (31) of a gas DE detector is better than 1%, even for very large entrance windows of several  $\text{cm}^2$ . This, of course, is not yet obtainable with very thin silicon detectors. Unlike solid-state detectors, the gas DE detector is not subject to radiation damage.

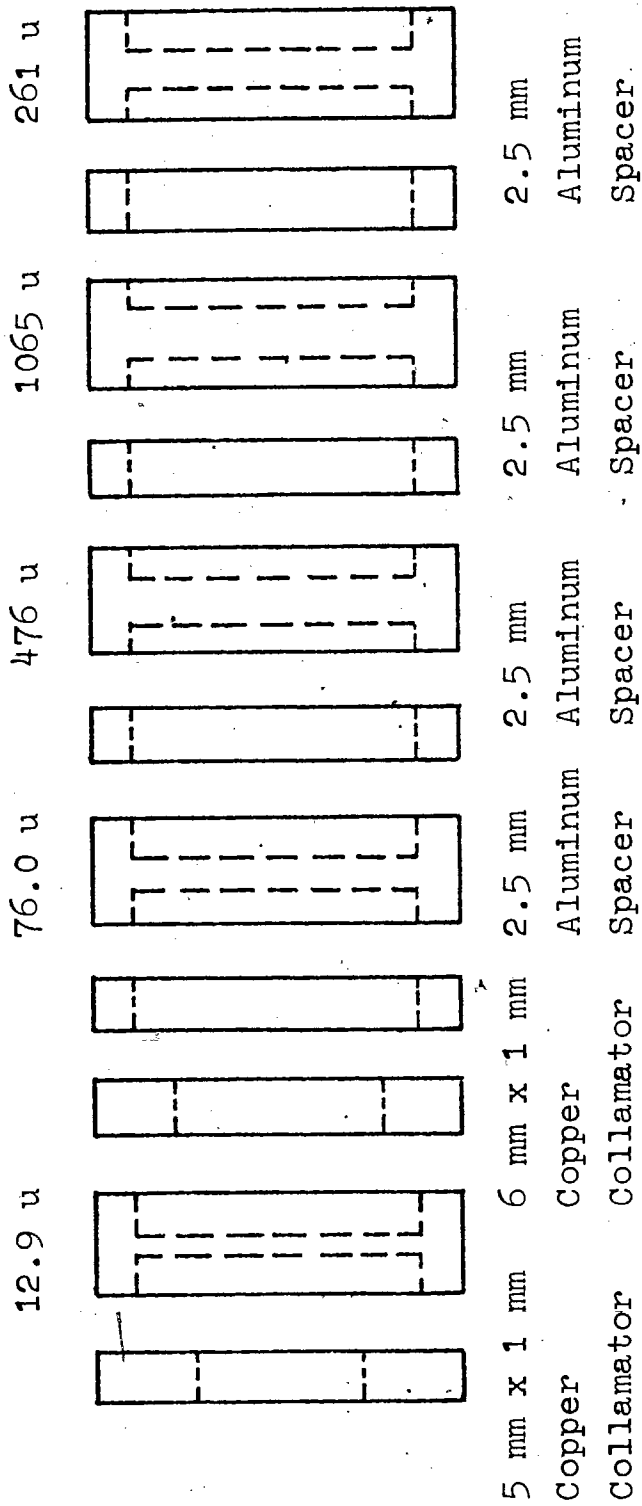
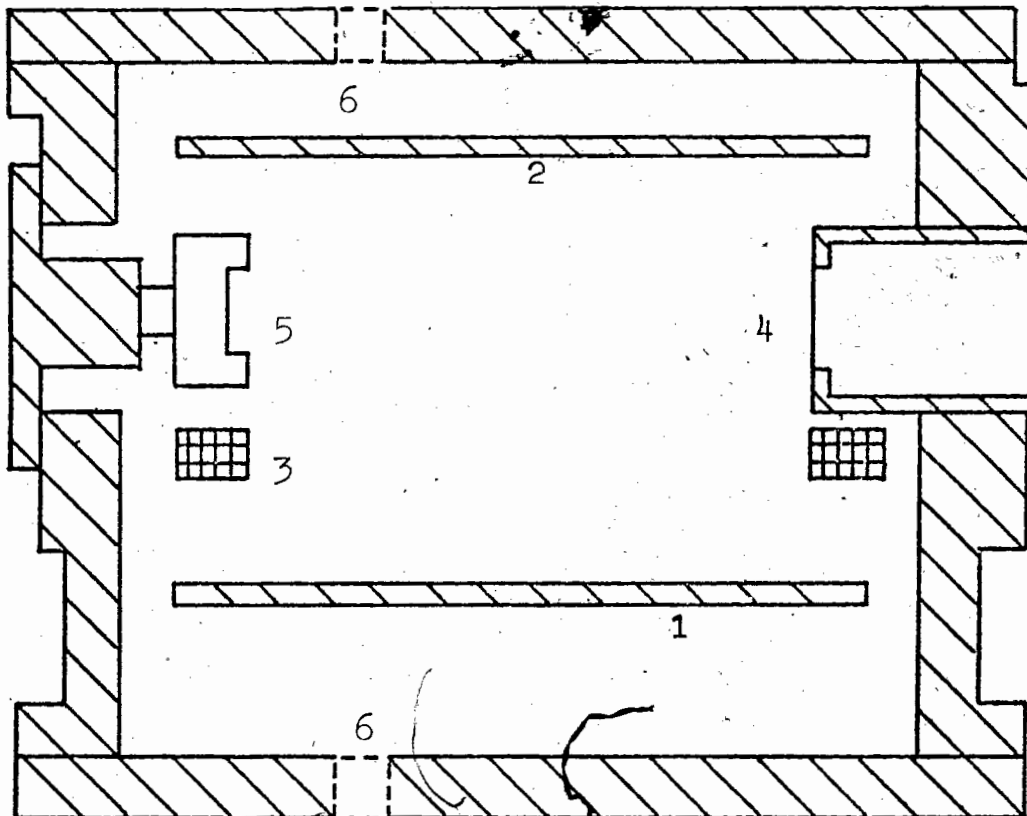


Figure 3. Detector stack orientation

Figure 4 illustrates the basic gas DE telescope as used by Barrette (31). The energy resolution of this telescope is comparable with that of a standard solid-state unit. Furthermore, the energy resolution of the gas DE detector is limited only by the straggling of the nuclear particles in the gas.

Recent advances in the production of thinner DE detectors have increased the mass region identifiable by the DE-E telescope. Detectors as thin as 10 microns are being produced with homogeneities of less than 5%. The use of these thinner detectors allows the identification of heavier particles,  $A \geq 16$ , providing that  $E_T/A > 2$  MeV/amu (31).

It is now the experimenter's responsibility to not only choose the correct detector configuration for his purposes, but to design and utilize a particle identification scheme which will make use of the improved energy resolution available.



- 1-- anode
- 2-- cathode
- 3-- Frisch grid
- 4-- entrance window
- 5-- solid state detector
- 6-- gas inlet and outlet

Figure 4. Gas DE telescope.

### 3.3: Particle Identification Methods

The following symbols will be referred to repeatedly in this section:

PI----- particle identification value

$A_i$ ----- mass of the charged particle in amu

$Z_{eff}$ ---- effective charge of the particle

dx----- thickness of the DE detector

$E_0$ ----- adjustable parameter to increase PI at low  $E_T$

k----- adjustable parameter to DE for optimizing resolution

a----- constant proportional to  $1/A_i Z_{eff}^2$

b----- adjustable parameter used in the power law expressions

<E>----- FWHM of the E signal

A variety of methods for the identification of nuclear particles from telescopic data is available. These include the use of identifier circuits, range-energy tables, and algorithms of varying complexity. This discussion is concerned with the latter two, as they provide the better resolution. The purpose, regardless of the method used, is to produce a nuclear particle identifier value, PI, which will be

constant for a given particle over a wide range of  $E_T$ . Furthermore, the method chosen must apply to the array of nuclear particles which is of interest to the experimenter.

In most instances, particle identification is accomplished through an algorithm. The multiplier form, which is based on the energy loss process, was commonly used in the beginning. Another, less restrictive form, uses the power-law relation, which relies on previously measured range data.

As we have discussed, the rate of energy loss due to ionization of a charged particle is described by the Bethe-Bloch equation:

$$\frac{dE}{dx} = -\frac{4\pi e^4 Z_i^2 N Z}{m_0 V^2} \left[ \ln \frac{2mV^2}{I} \right] \quad 18.$$

In contrast to equation (7) several simplifications have been made. In the majority of nuclear particle identification studies, the ions are non-relativistic, therefore those terms involving  $\beta^2$  were eliminated. Furthermore, in the case of most algorithms, the electron shell non-participation term,

$C/Z$ , as well as the density correction term  $\delta/2$ , are left out as their effects are assumed to be small. The use of this simplified form of the Bethe-Bloch equation was the basis for the early multiplier algorithms. From the arguments given in equations (28) and (29), the general form may be expressed:

$$(E + dE)(dE) \propto A_i Z_{\text{eff}}^2 dx \quad 19.$$

where  $A_i$  is the mass of the charged particle,  $Z_{\text{eff}}$  is its effective charge, and  $dx$  is the thickness of the DE detector. However, this particular form was not satisfactory as it failed to apply to a broad range of particles and energies. The most serious problem involved the deviation of the PI value, which increased as a particle's energy decreased. This was partially alleviated by including a factor,  $E_0$ , in the  $E_T$  part of the relation:

$$(E + dE + E_0)(dE) \propto A_i Z_{\text{eff}}^2 dx \quad 20.$$

The effect of this correction is illustrated in Figure 5. Despite this alteration it was still necessary to

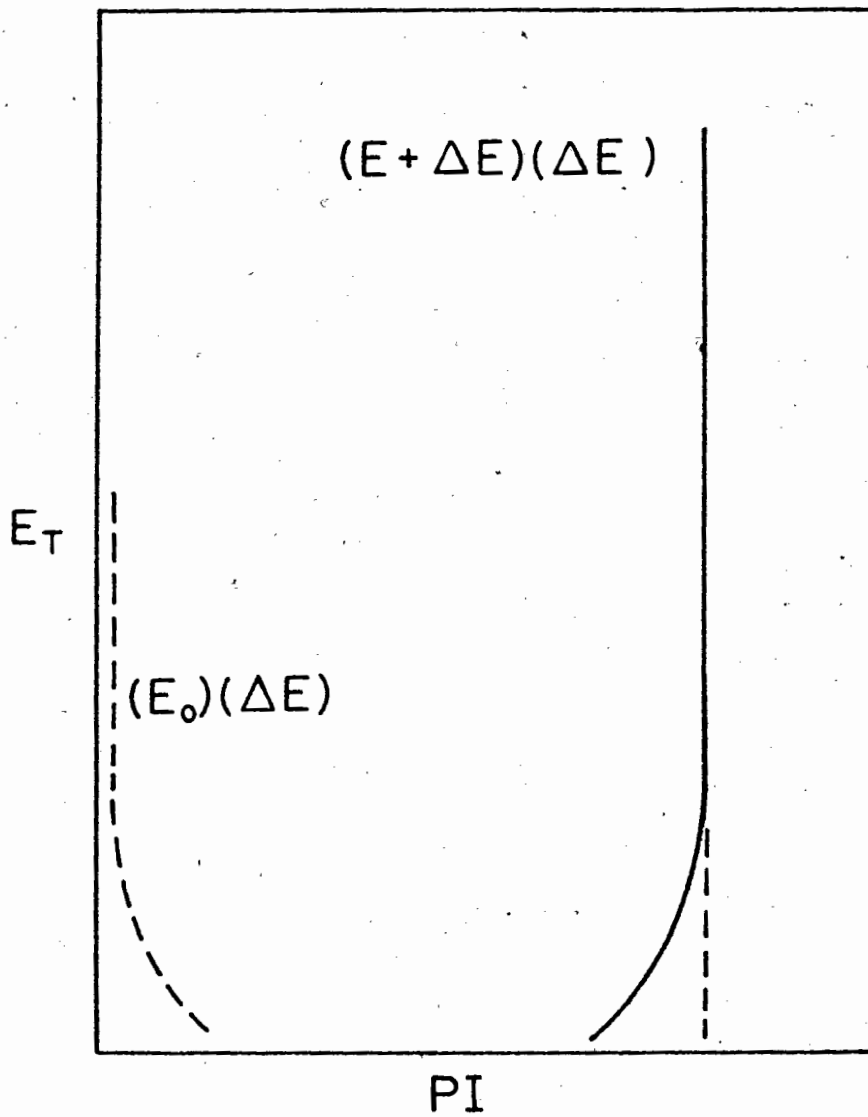


Figure 5. The effect of including the arbitrary  $E_0$  correction in the multiplier algorithm.

include another adjustable parameter  $k$ , which would alter the value of  $dE$  to give the best particle resolution. This gave a multiplier algorithm with the following form:

$$(E + dE + E_0 + k dE)(dE) \propto A_i Z_{\text{eff}}^2 dx \quad 21.$$

The necessity for these adjustable parameters limits the effectiveness of these algorithms. For this particular reason, the majority of the telescopic data analyses use a power-law based algorithm which has the general form:

$$\text{Range} = a E_T^b \quad 22.$$

where  $1/a$  is a constant which approximates  $A_i Z_{\text{eff}}^2$  and  $b$  is an adjustable parameter which decreases as  $Z$  increases. For nuclear particles obeying the range expression, it can be shown that:

$$\left[ (E + dE)^b - E^b \right] = \frac{dx}{a} \quad 23.$$

Since  $dx$ , the thickness of the DE detector, is known and  $E$  and  $dE$  are measured, it is possible to determine  $A_i Z_{\text{eff}}^2$ . Butler, Poskanzer, and Landis (32) used a modified version of the power-law relation:

$$PI(\text{particle identification}) = \left[ \frac{(E+dE)^n}{k} - \frac{(E)^n}{k} \right]^{1/2} \quad 24.$$

where  $n = b - CdE/x$ .  $C$  and  $k$  are constants with  $C$  in  $\text{mg.MeV/cm}^2$  and  $k$  is set equal to 300. This particular expression is capable of automatically adjusting the value of the exponent, resulting in improved resolution for a wider range of particles. The exponent has been set to decrease with the value of  $dE$  since the heavier nuclei with the lower energies, which deviate most from the power-law relation, have the higher energy losses in the DE detector. Bowman et-al (36) modified the algorithm further, so that the exponent decreases linearly with  $dE/E$  rather than  $dE$  only. This form of the expression further increased the applicability of the DE-E method. However, Korteling, Toren, and Hyde (37) found that an alternative approach gave a higher degree of resolution when a thin 16 micron DE detector was used. Relying on the Bethe-Bloch expression, they

generated the following algorithm:

$$PI = \left[ k (E_T / \ln E_T) (E/1024)^b \right]^{1/2} \quad 25.$$

where  $k = (\ln 1024 / 1024)^{1/2} (1024)$ . The presence of the 1024 factor in this constant as well as in the denominator of the expression is related to the initial scale in which the input data was collected. The square root operation allows PI to follow Z more linearly, while the exponent b is a correction for certain approximations to the particular Bethe-Bloch expression originally used. This exponent is given a value of 1.0 for the lighter elements, Z up to 4, and it increases exponentially with Z resulting in a value of 10 for Z = 18.

A second technique consists of storing a range-energy table in a computer and using it to calculate an apparent thickness of the DE detector for each event registered in the telescope. If the calculated thickness corresponds to the true thickness, a peak will result indicating the particle involved. Recently, Chulick (38) devised a scheme utilizing the tables of Northcliffe and Schilling. Determinations

with this method were limited to  $Z \geq 4$ , however.

Other algorithms have been developed using similar approaches, however neither their resolution nor their applicability exceeds those schemes already mentioned.

Inspection of the expressions already presented suggests that any deviation in the determination of  $dE$  or  $E$  will tend to limit the resolving power of the algorithm in use. Figure 6 (30), expresses the degree of accuracy necessary to resolve isotopes with  $Z < 10$ , when relying on calculations of  $A_i Z^2$ . It is apparent that a deviation of only 5% in  $MZ^2$  can disrupt isotope resolution for particles with  $Z > 3$ . Furthermore, for lithium and above, there is a definite overlap of  $MZ^2$  for the neighboring isobars. For example, a 5% deviation in the determination of  $MZ^2$  will make  ${}^6\text{Li}$  unresolvable from  ${}^7\text{Li}$ . Furthermore, there would be no distinction between  ${}^{11}\text{Li}$  and  ${}^7\text{Be}$ . Note also that, for  $Z > 6$ , errors in  $MZ^2$  as low as 1% will inhibit all isotopic resolution. Therefore, it can be seen that even very small fluctuations in the  $dE$  or  $E$  signals can result in poor resolution. Several factors can contribute to these errors, although the majority

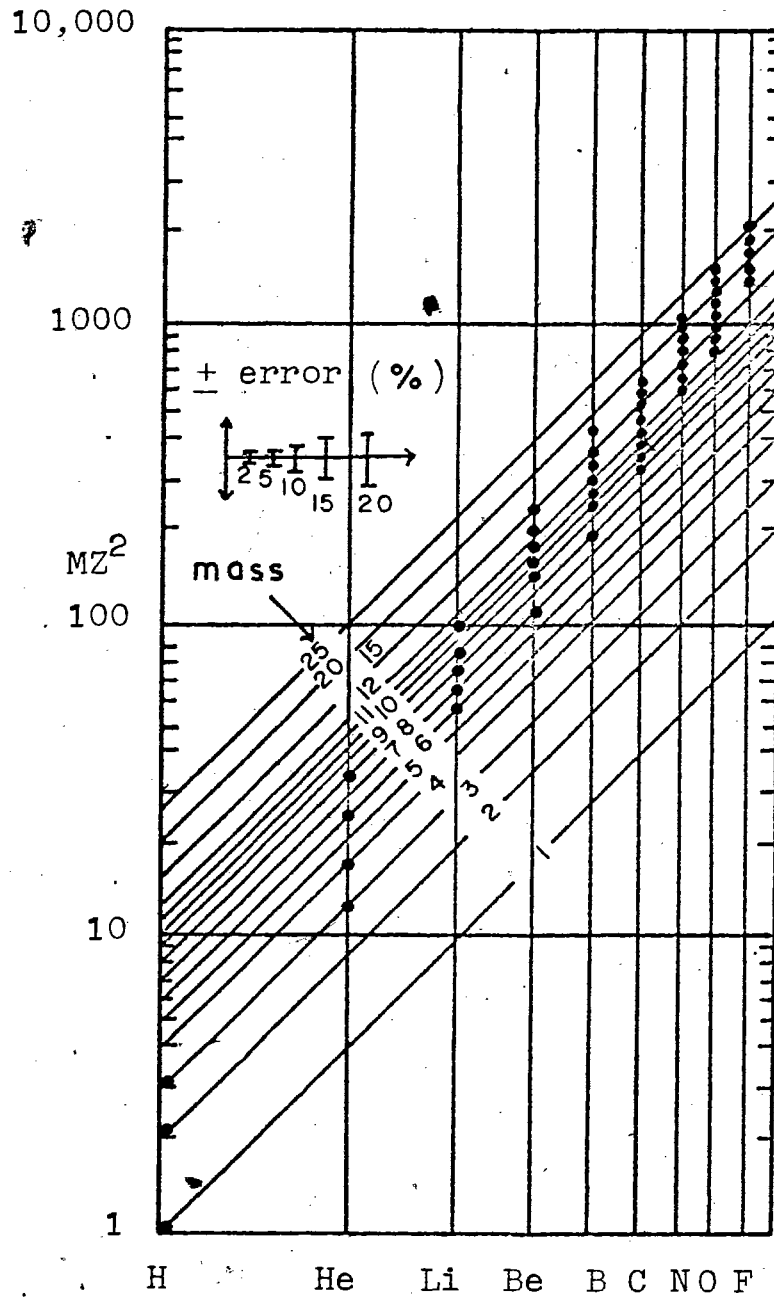


Figure 6. Plot of  $MZ^2$  for ions of  $Z < 10$ , known to be stable against particle break-up.

involve some process in the DE detector.

Electronic noise arising from the high capacitance of the DE detector can play a major role when DE signals are very low. However, the overall electronic noise, ranging from 30 keV and above, has little effect on the resolution of general telescope studies.

Although virtually eliminated by proper detector construction, channeling could contribute a significant source of error, due to the deposition of less energy than would normally be expected.

For low energy ions, charge pick-up can produce energy loss deviations in the DE detector. This factor becomes increasingly important with the use of thinner DE detectors which allow observation of low energy particles with  $E_T < 1 \text{ MeV/amu}$ . Of course, no problem exists with high energy particles as they remain stripped until they reach their range in the E detector.

Straggling is a major source of energy loss fluctuations in the DE detector. As previously

described, the degree of this effect depends on the relative thickness of the DE detector when compared to the energy of the nuclear particle. With the availability of thinner DE detectors, homogeneity becomes increasingly important, as variations in thickness can cause considerable energy loss fluctuations for low energy ions. Fortunately, those detectors available on the market are produced under exacting conditions which result in satisfactory uniformity.

Although the major problems involve the DE detector, instances do exist where the fluctuation in the energy deposition in the E detector becomes important. When a charged particle has lost sufficient energy, it will pick-up electrons until it becomes neutral. At this point, nuclear collisions become the dominant mode of energy loss as described by Lindhard and Nielson (39). Deviations in these interactions can result in an increase in the width of the energy loss in the E detector, where the FWHM is given by:

$$\langle E \rangle = 0.7 Z_i^{1/2} A_i^{4/3} \text{ keV}$$

This width is small for protons, around 0.70 keV, however it increases for heavier ions. In the case of  $Z = 10$ , the width can exceed 100 keV, which is significant for those particles that just enter the E detector and deposit very little energy. For these same type of particles, the dead layers on the back of the DE and on the front of the E detector can cause deviations in the E signal. For this reason it is important to minimize the thickness of the Au and Al dead layers. Both the Au and the Al dead layers on the detectors in this study, were 40 micro-grams/cm<sup>2</sup>.

With the availability of thinner silicon surface barrier detectors with increased energy resolution and uniform thicknesses many of the restrictions to particle resolution have been eliminated. Although the state-of-the-art of particle identification has been enhanced by the advent of newer, more complex empirical relations, its full potential has yet to be realized. Any advances in the particle resolution by the DE-E technique will require the solutions to those problems presented in this section.

#### 4.0: EXPERIMENTAL PROCEDURES

##### 4.1: Physical Configuration

The nuclear particles studied in this investigation were produced by proton bombardment of a silver foil. The thickness of the target was nominally 1 mg/cm<sup>2</sup>. This is sufficiently thin to allow the escape of low energy heavy ions, well below the range limit of the thinnest DE detector used. The target is also thick enough to produce a reasonable counting rate in the detectors.

The protons were produced by the TRIUMF cyclotron, with specific energies ranging from 200 to 480 MeV. The extracted beam currents extended from 50 to 200 nano-amperes, while the focused beam spot on the target was approximately 1 cm. in diameter.

All experiments were carried out in the 60 inch Simon Fraser University scattering chamber, which is located on the floor of the proton hall at the facility. This particular chamber contains four moveable arms and one multiple target ladder, all of which are remote controlled from the experimenter's

station located approximately 100 feet away. The pressure in the chamber was held at approximately  $5 \times 10^{-6}$  torr by a turbomolecular pump.

Telescopes containing from three to five detectors were employed in this study. The configurations utilized are described in Table II. Although the three detector telescope is less complicated to use, the five detector unit allows increased versatility. By careful planning, the various detector thicknesses may be chosen in such a manner as to facilitate the broadest range of particles and energies observable by the telescope. This is made possible by assigning from one to three adjacent detectors as the DE, prior to the final analysis. In this manner, the data from one five detector telescope may be analyzed as that taken from three separate telescopes.

Independent of the final configuration chosen, the resultant detector block is mounted on one of the arms, 25 to 35 cm. from the target. At 35 cm., the solid angle was  $1.60 \times 10^{-4}$  sterads. With a beam current of 200 nano-amperes, approximately 200 valid events/sec were recorded by the telescope.

Fragment measurements were made at 20, 90, and 160 degrees, with the target positioned at 125 degrees to the beam.

Table II: Telescope Configurations

Position	Sensitive Depth (microns)	Range (MeV)
=====		
A. Configuration 3-A		
DE	33.8	0 - 30
E	1065.	0 - 100
E-Reject	210.	> 0.4
C. Configuration 5-A		
F-1	12.9	0 - 25
F-2	76.	0 - 90
F-3	476.	0 - 180
F-4	1065.	0 - 150
F-5	161.	> 0.4

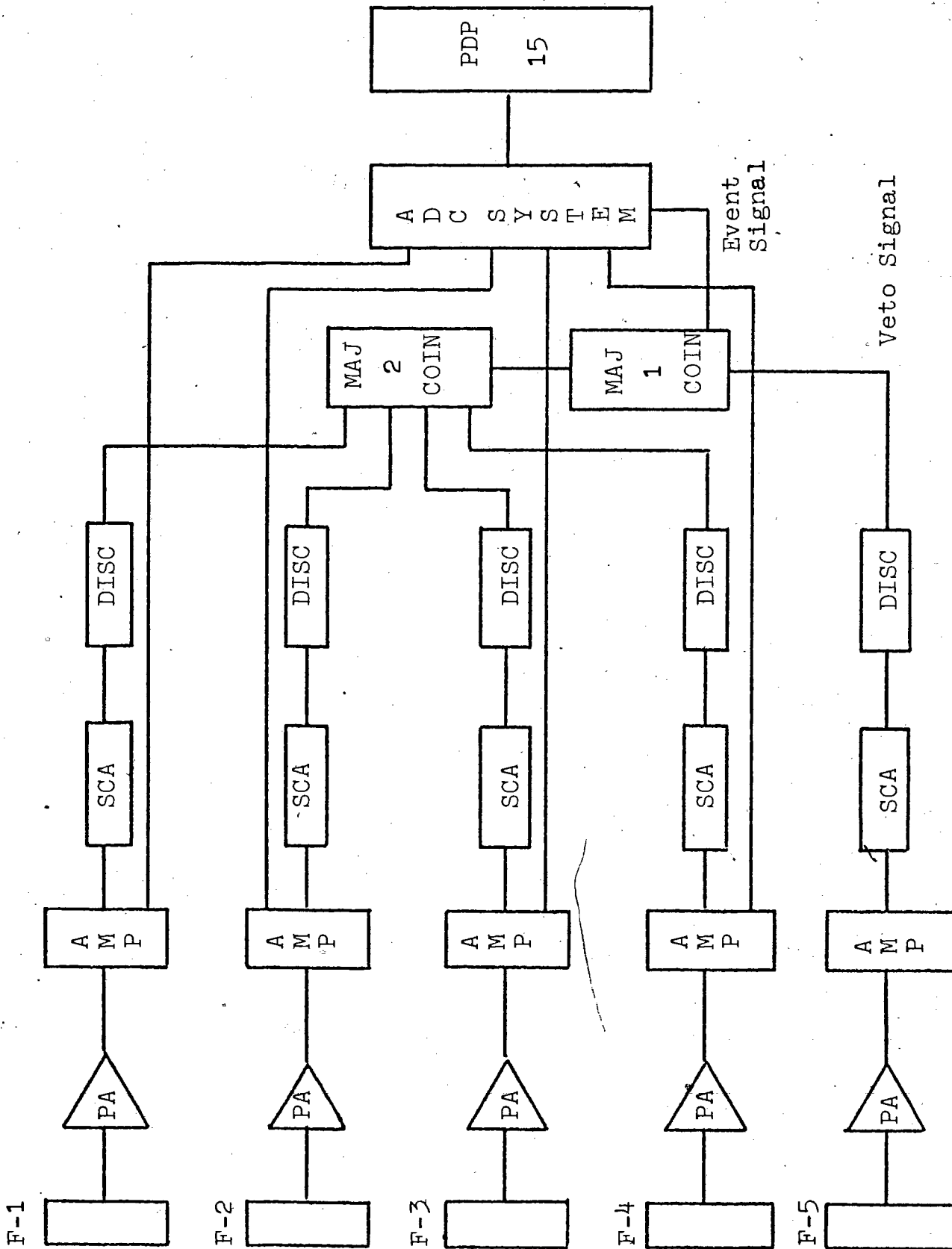
#### 4.2: Electronics

The following discussion describes the basic electronic system employed. A schematic diagram for the five detector system is shown in Figure 7.

All of the electronics described were separated from the scattering chamber by approximately 100 feet of 93 ohm shielded cable, except for the preamplifiers which were located at the chamber. The preamplifiers were separated from the detectors by five feet of microdot cable, located inside the chamber, followed by 12 inches of 93 ohm cable on the outside. The energy signals from the preamplifiers, resulting from the energy deposition by charged particles in the detectors, were processed by delay line amplifiers. Each delayed unipolar output was delayed further by 1.25 micro-seconds before entering the data acquisition system, which will be described later in more detail. This delay is necessary, in order that sufficient time is provided for the logic decisions to be made which will allow or terminate any further processing of the signals by the data acquisition system.

The prompt bi-polar outputs of the amplifiers

Figure 7. Electronics for a five detector system



were sent to timing single channel analyzers. These units were set to accept only a predetermined energy range of signals. The resultant timing output may also be delayed as required for coincident logic decisions. An example of the energy ranges allowed for each detector in the telescope is given in Table II. These particular ranges were determined by a program, titled LAZY (40), which depends on the range-energy method of Stewart (41). It calculates the energy lost by any number of different fragments in each detector of a stack. Output is received over an energy range for each type of particle, based on the required energy to just enter the first detector up to that necessary to just exit the final detector.

The delayed signals from the single channel analyzers were sent to updating discriminators which allow both a width adjustment and a source of identical multiple outputs for each input. The widths of the DE and E signals were set at 60 nano-seconds for later coincidence overlap processing, while the E-reject signal, used to veto a coincidence, was set at 100 nano-seconds. Majority two logic was used in the coincidence unit to sort coincidences from the incoming signals.

#### 4.3: Calibration

Calibration was carried out prior to each set of experiments. First, each detector was normalized to a precision pulse generator, using the 8.785 MeV alpha from a ThC' source. Although the range of this alpha particle is 55 microns in silicon, we have found it useful for much thinner detectors. A significant number of alpha particles are Rutherford scattered by the gold dead layer of the detectors. This increases the available range of the particle in the detector such that the total energy of the alpha is deposited, rather than just a fraction. This results in the accumulation of the full energy peaks of ThC' in a reasonable counting period. This method has proven more convenient and accurate than determining the deposited energy by relying on the measurement of the residual energy of the non-scattered alpha particles in a second thick detector.

The calibration steps were completed using the same cables and electronics as were used in the normalization. By setting the pulser to the previously determined normalized settings for each specific detector, calibration spectra can be collected by

counting sufficient pulser peaks to cover the particular energy range of each detector. Later, these peaks were fitted by a linear least squares program, which generates a slope and intercept to be used in the final analysis. The points used in the calibration were normally within one part in 2000 of the calculated curve.

#### 4.4: Data Acquisition System

The original delayed signals from the amplifiers and the event signals generated by the logic system are sent to an eleven bit stretcher multiplexor-ADC system, interfaced to a PDP-15 computer. The basic hardware of this system allows simultaneous processing of data from several independent detectors as well as complex multiparameter arrays.

The PDP-15 utilizes a multi-purpose pulse-height analysis program, named FOLDAP, to handle the incoming data. Prior to each set of experiments, an analyzer configuration is designed and fed into the computer. This defines the on-line data monitoring

operations of the twelve available video displays. Singles, as well as coincidence spectra are observed throughout each experiment. Not only does this offer the experimenter the chance to confirm the proper operation of his detectors and electronics, but allows him to monitor the particle and energy ranges observable by the system. Measurements proportional to the beam current are collected in time bins of 2 to 5 minutes and are available as a video display also. Several Camac controlled scalers exist for integrated data rate information as well. Valid events are collected in blocks of 256 which are written onto 9 track magnetic tape for further off-line analysis.

#### 4.5 Off-Line Data Analysis:

The recorded data is processed by a series of programs at the IBM 370 facility located at Simon Fraser University.

The raw data is initially sorted by the program SORT. Basically, this separates the events of interest from the recorded data, and transfers them onto a new tape. Several important functions are performed in this operation, including the digital stabilization of

the collected data. The pulser events are counted as a function of time as well. From the resultant time-based plots generated, the quality of the data may be checked. This feature allows any questionable time blocks of data to be disregarded in further analysis.

The sorted data is analyzed, event-by-event, using the program ANAL, which contains a particle identification algorithm. The telescopic configuration is specified at this time. When analyzing data from a five detector unit, there are three choices for the DE thickness, therefore this program would be run three times in order to extract all of the available information.

The PI output is available in several forms, including PI spectra as well as two dimensional displays of PI verses dE, E, and  $E_T$ . Several other options are available for passing histograms of PI on to separate programs designed for cross-section analysis and graphical display.

The programs and options used in this study will be described in more detail in the following section.

## 5.0: RESULTS OF STRAGGLING MEASUREMENTS

With the beam currents available at TRIUMF, sufficient statistics were accumulated for an in-depth analysis of straggling for protons of 2 to 14 MeV/amu and for alpha particles of 2 to 7.5 MeV/amu. DE detector thicknesses of 76 and 476 microns were used in the proton study, while 12.9 and 33.8 micron DE detectors were used in the alpha particle investigation.

From the energy range of each particle and the specific DE thicknesses used, one may calculate the Vavilov parameter  $K$ , from equation 12. This value indicates in which theoretical region a particular set of measurements belong. For all of the studied cases,  $K \gg 1$ . Therefore Gaussian distributions may be assumed, and Tschalar's calculations (20,21,22) are expected to be valid.

Using the program ANAL, a matrix of E-Total verses dE for each experiment was constructed. From this basic matrix, windows were set on specific values of E-Total. The resultant histogram was then processed by a subroutine called PEAKFITTER which fits each

occurring peak to a Gaussian distribution. This was accomplished by generating chi-squared values for several fits from 10% on either side of the centroid. The fit with the lowest chi-squared value was chosen and stored.

Each peak found represented the distribution of energy losses of a particular charged particle at that value of E-Total which had been specified. Next, the associated FWHM of each peak was calculated and printed along with other parameters of interest. The chi-square values for the chosen fit and for 10% on either side were listed as a check of the symmetry of each distribution.

### 5.1: Proton Straggling

The measurements of proton straggling in 76 and 476 micron DE detectors are presented in Figures 8 and 9. The 76 micron case was derived from a single experiment, while the distribution from the 476 micron case was taken from four identical experiments to insure reproducibility. In the latter case the correlation coefficients of the combined data were greater than .850, as calculated by the method



Figure 8 Proton straggling in a  
 $76\mu$  Si detector

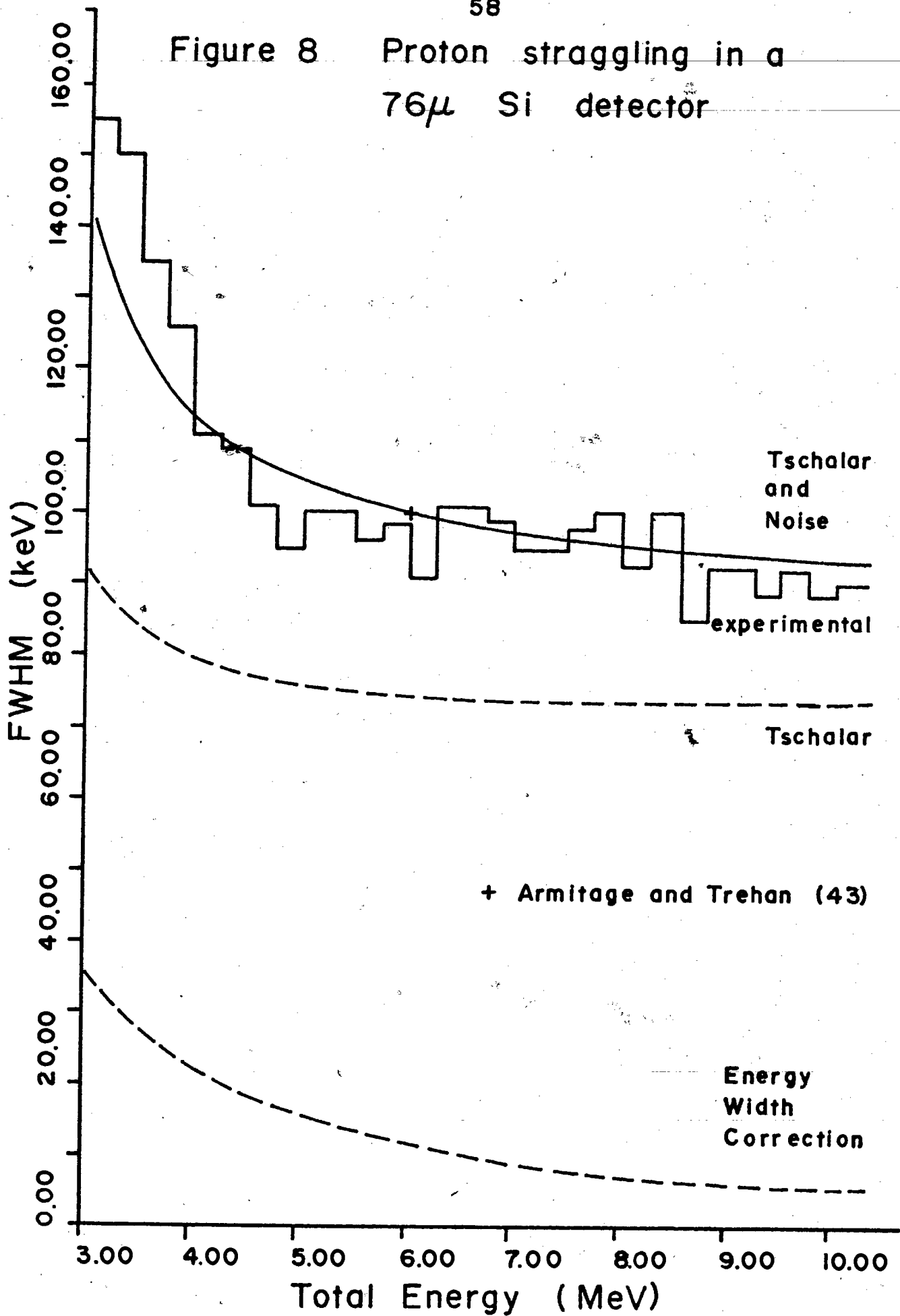
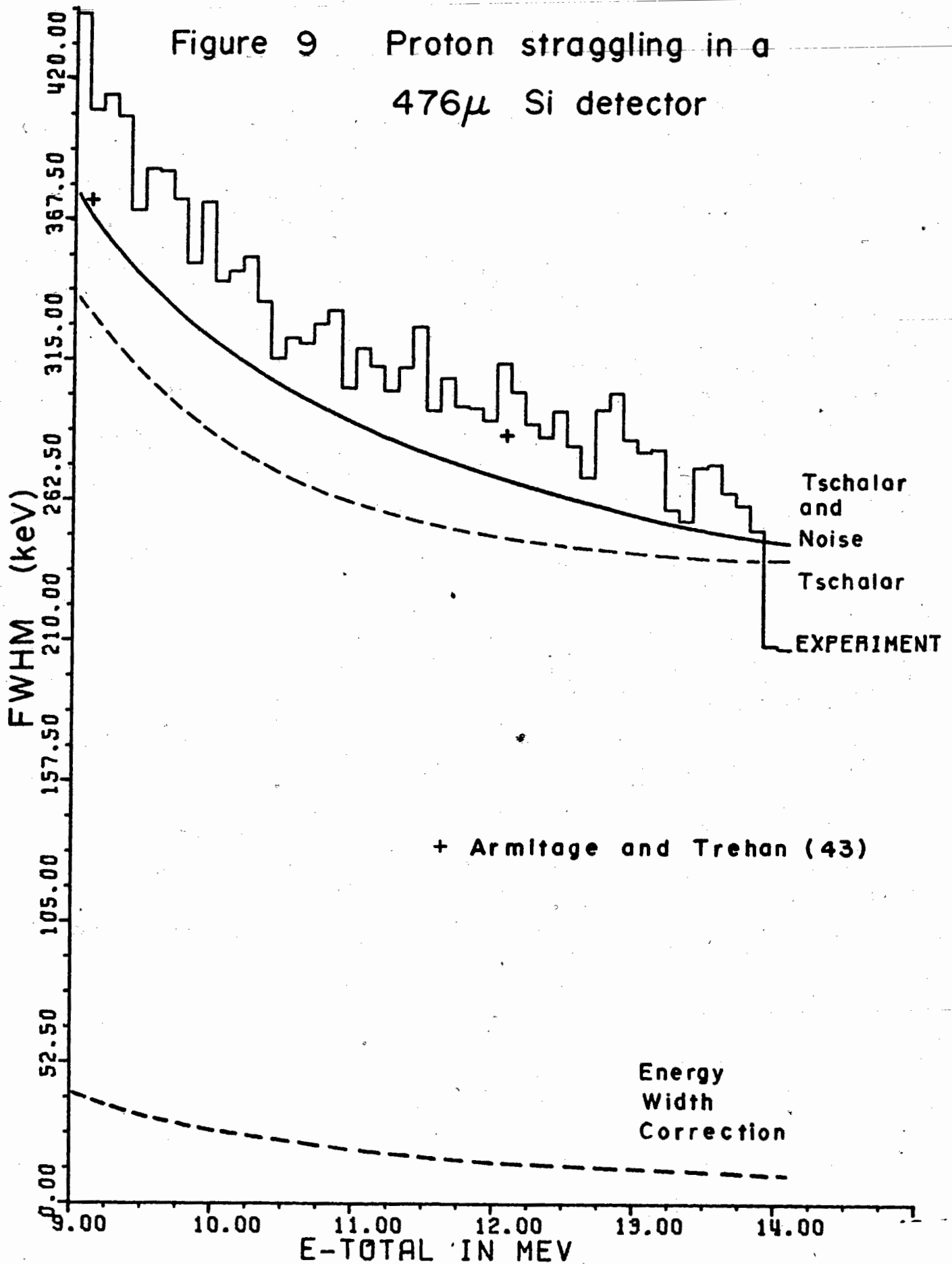


Figure 9 Proton straggling in a 476 $\mu$  Si detector



described in Appendix A. The measured values include detector and electronic noise. A correction is also indicated for the increase in the measured width caused by the fixed window size used in each particular analysis.

Using the relationships of Tschalar (20,21,22); theoretical distributions were calculated. The results are included in the figures. Measurements made by Armitage and Trehan (43) are included for comparison.

In the case of the 476 micron DE detector, the theoretical predictions of Tschalar follow the experimental values closely. However, the theoretical values are low by a factor of approximately 10%. The values measured by Armitage and Trehan (43) were high by 20%. In the 76 micron study, the theoretical predictions agree with the measured values within statistics.

## 5.2: Alpha Particle Straggling

The straggling measurements for alpha particles incident on 12.9 and 33.8 micron DE detectors are presented in Figures 10 and 11. The 12.9 micron

Figure 10  $^4\text{He}$  straggling in a  
 $12.9\mu$  Si detector

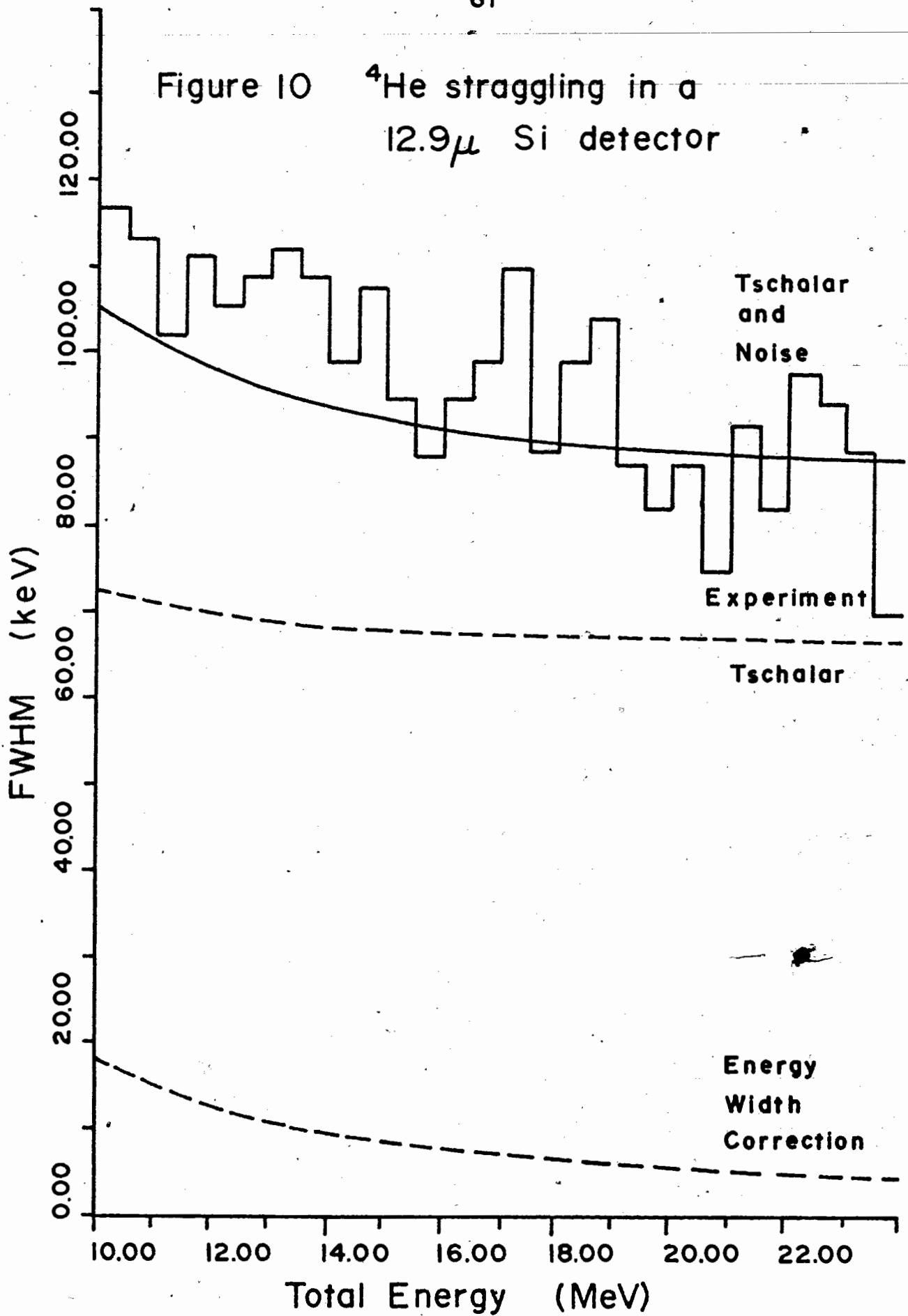
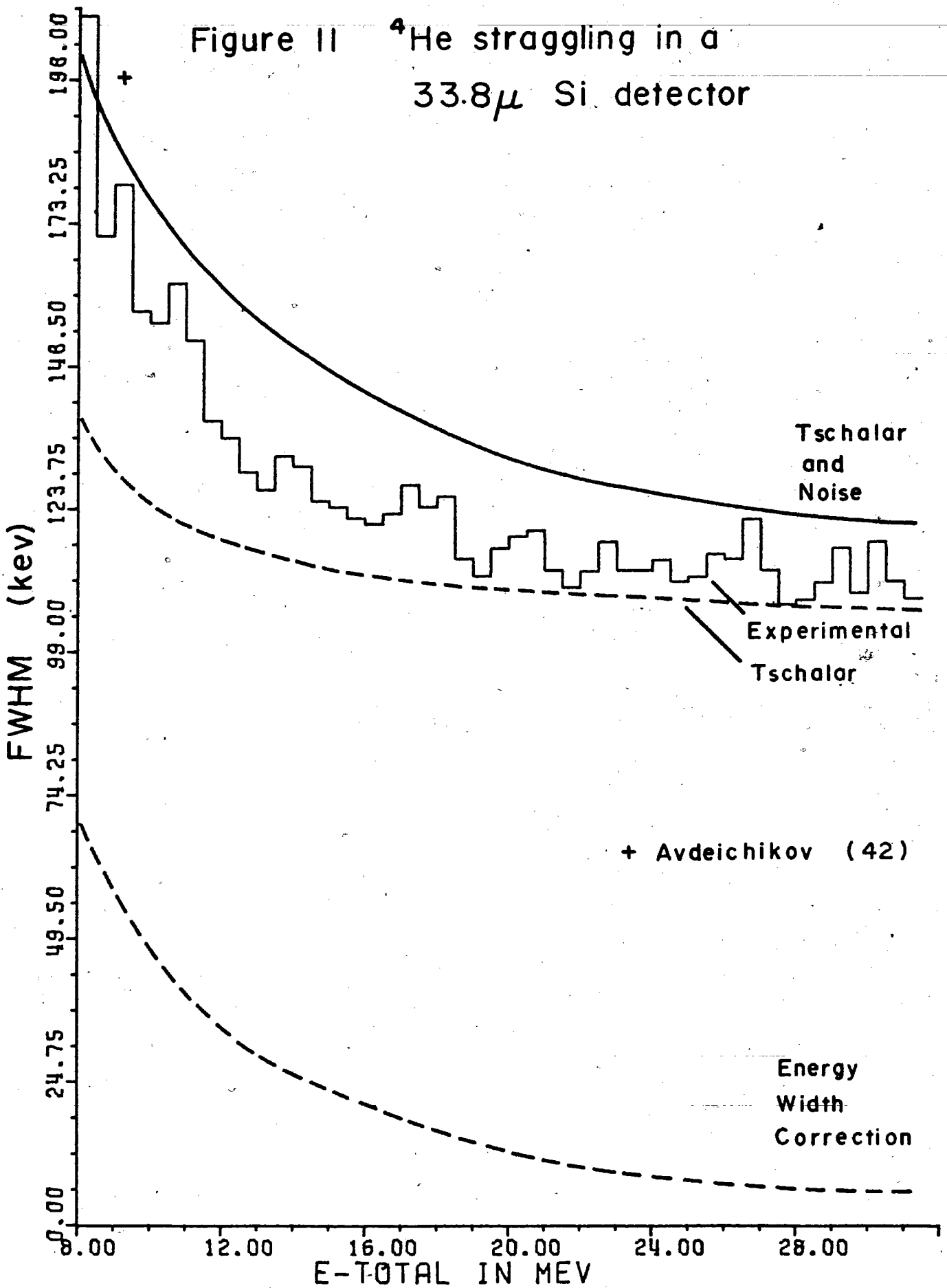


Figure II  $^4\text{He}$  straggling in a  
 $33.8\mu$  Si detector



distribution was taken from three identical experiments with correlation coefficients greater than .940. The distribution for the 33.8 micron case was derived from a single experiment.

Both experimental distributions include detector and electronic noise. Tschalar's relations are valid for both of the alpha studies and were used to calculate the theoretical straggling curves presented in the figures. Data from the study of Avdeichikov (42) is included for comparison.

The agreement of the measured values with the theoretical predictions is good in the 33.8 micron case although the calculated values are high by 10 to 15%. Avdeichikov (4) found his measured values were 20% higher than they calculated when he studied 8.78 MeV alpha particles incident on silicon absorbers of varying thicknesses. In the 12.9 micron study, the theoretical agreement is good within statistics.

#### 5.4: Theoretical Problems

Although there was general agreement between the measured and calculated widths in this study, other

groups have observed some disagreement. A brief discussion of the inconsistencies of Tschalar's expressions is necessary to explain the occurrence of these deviations.

The disagreement between the measurements and the values predicted by Tschalar's calculations, for those particles in the lower energy range, may be explained by the presence of non-statistical fluctuations. The expressions of Tschalar assume that the particle is completely ionized during its passage through the absorber. However, at particle energies of  $\leq 3$  MeV/amu, charge state fluctuations may begin to occur, as discussed by Schmidt et al (44). This process does not give rise to discrete charge groups, but produces a broadened distribution instead. The broader the ionic charge distribution and the smaller the frequency of charge altering processes, the more the charge state fluctuations contribute to the energy straggling. However, since the low energy regions investigated in this study border on 3 MeV/amu, little deviation is observed between the measured and calculated values. The addition of this correction to Tschalar's expressions would be a logical and worthwhile step towards a more consistent means of

predicting energy loss distributions at low particle energies.

The general disagreement of the theory over the remaining energy range has been discussed by Armitage and Trehan (43). Originally, Tschalar ignored atomic binding of interacting electrons by assuming that the velocity of the particle was greater than the velocity of its own orbital electrons as well as greater than those of the absorber, which is not always the case. For example, at 5 MeV/amu, both protons and alpha particles have a velocity equivalent to the K-shell electrons of silicon. By altering the single collision cross section, which is a major feature of Tschalar's approach, in order to take into account the atomic binding of the interacting electrons, one can enhance the agreement with Tschalar's predictions to some extent.

Tschalar and Maccabee (22) increased their straggling values by 9% to take care of atomic binding, with good results. However, in the cases they were studying, widening by atomic binding was < 3%. Avdeichikov (42) included this correction by increasing the average ionization potential of silicon by 10%.

However his measured results were still high by 20 %. Kolata and Amos (45) obtained good agreement with Tschalar's calculations for 5 and 7 MeV protons incident on silicon without introducing any correction.

The theoretical values presented in this study were calculated without regard to atomic binding, with varying results. A re-evaluation of the form of this correction is in order. The current method of increasing the value of the ionization potential of the absorbing material over the entire energy range of the particle is not satisfactory. A more suitable correction would involve an expression for the ionization potential which varied with particle charge and energy.

#### 5.4: Optimization of the DE-E Technique

As previously discussed, the resolution of the DE-E system is limited by straggling, with the effect in the DE detector dominating the interference. If different particles of the same incident energy have overlapping straggling curves in this detector, it will not be possible to identify those particles having energy losses in the region of overlap.

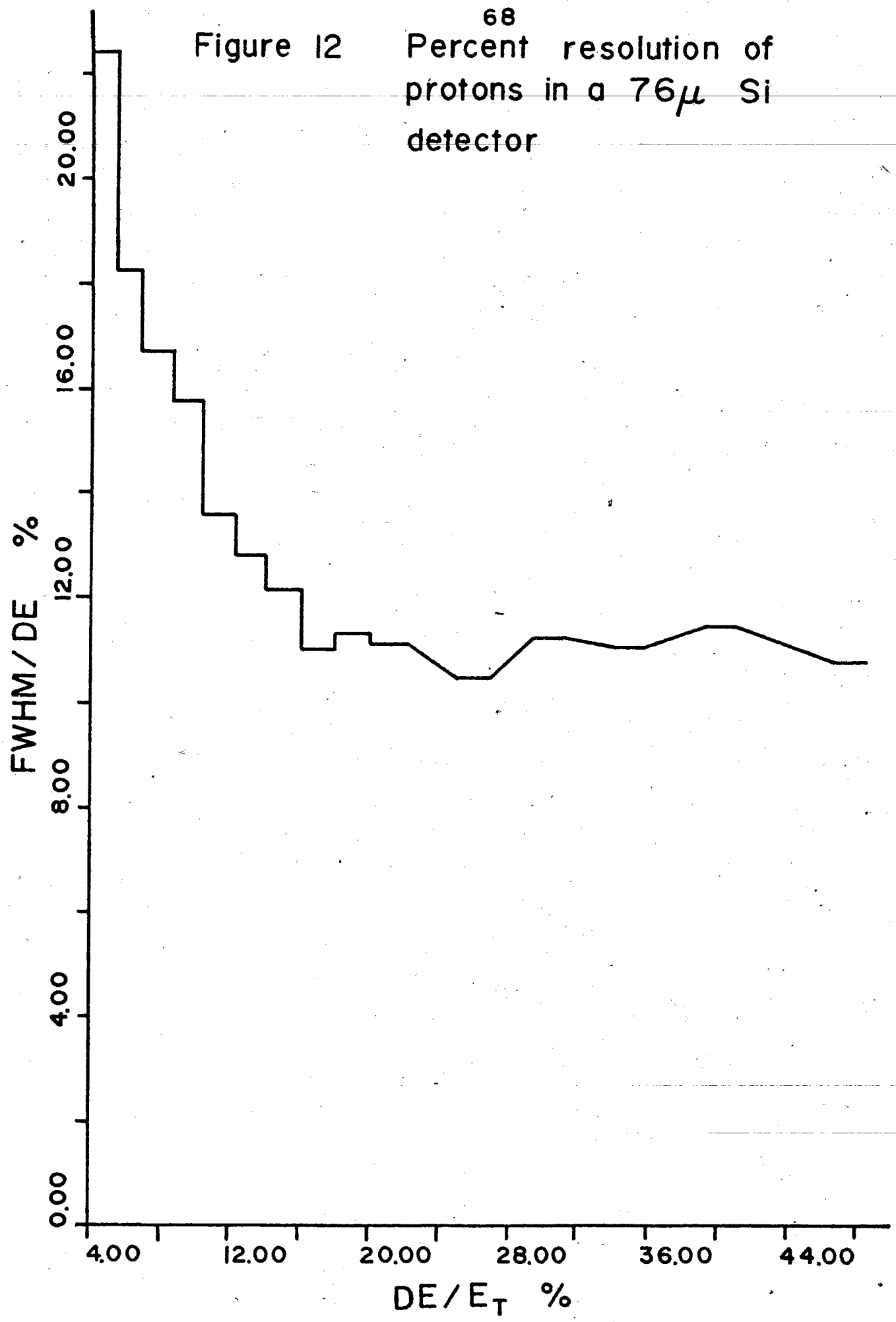
Measurements, of the type presented here, are not only useful for the study of the penetration of charged particles through matter, but can indicate under what conditions overlapping straggling curves occur. With sufficient similar information, telescopic configurations may be chosen which will optimize particle identification.

For our purposes, the absolute value of the straggling width is not a convenient parameter, as it does not indicate the actual energy resolution of the DE detector. Following the procedure of Avdeichikov (42), the straggling width is plotted, combined with the measured energy deposited by the particle in the DE detector. This function,  $\text{FWHM}/\text{DE}\%$ , represents the actual percent resolution.

By plotting this value against the percent energy dropped in the DE detector, one may observe those regions where optimum energy resolution is achieved.

The measurements of proton straggling with a telescope utilizing a 76.0 micron DE detector are presented in Figure 12. The percent resolution is

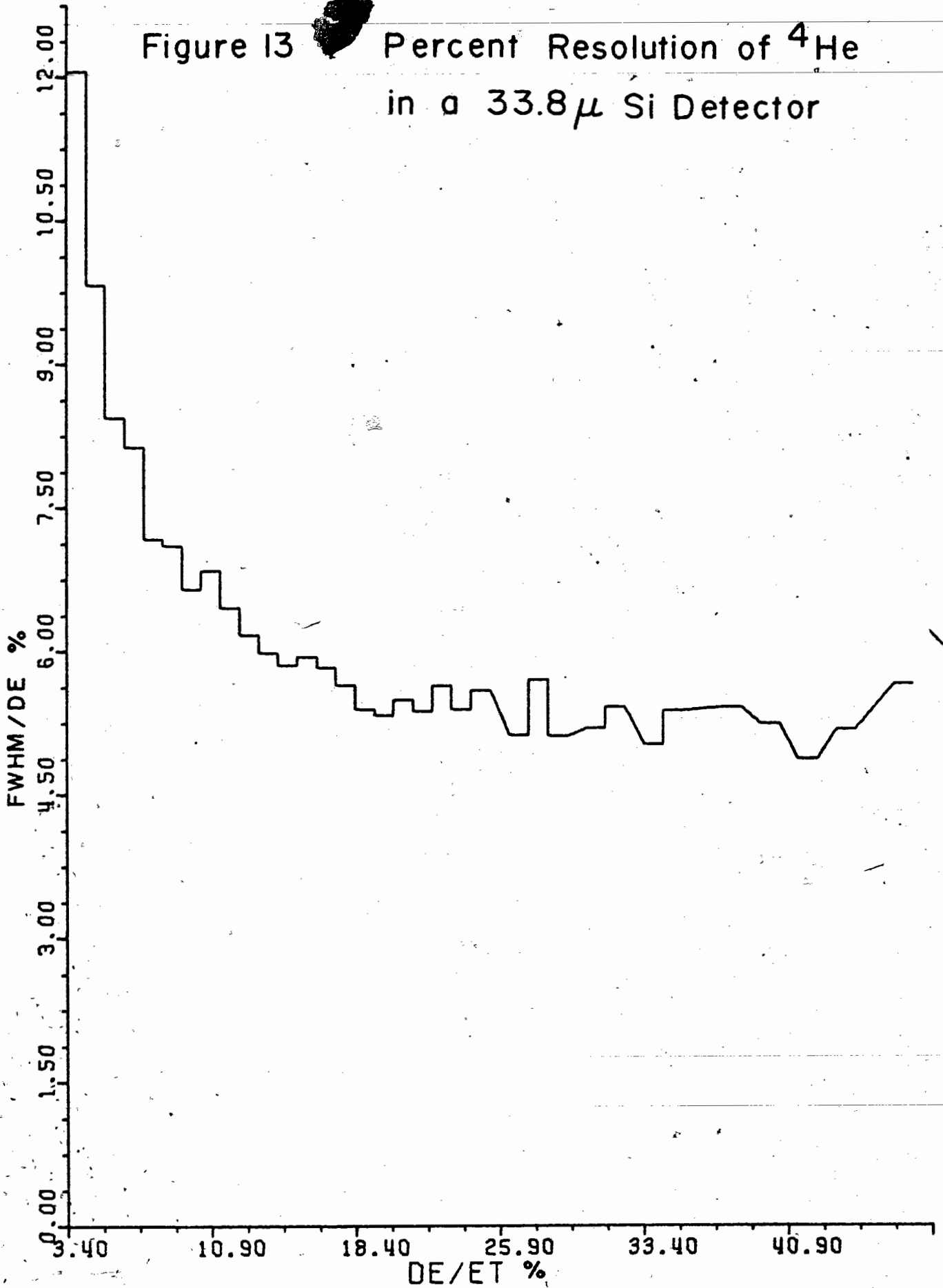
Figure 12 Percent resolution of protons in a 76 $\mu$  Si detector



observed to decrease to a constant value, within statistics, at an energy loss of 20%. This trend continues to the end of the measured data, corresponding to an energy loss of approximately 50%.

In a similar manner, the measurements of alpha particles incident on a 33.8 micron DE detector are presented in Figure 13. Again, the percent resolution is observed to decrease to a constant value, at an energy loss of 15% in this case. The value of the percent resolution remains constant throughout the rest of the measured range to an energy loss of approximately 50%. Avdeichikov (42) reported a similar trend in his study of 7.70 MeV alpha particles incident on silicon absorbers. However, his reported measurements of the percent resolution reached a constant value at an energy loss of 30%.

Figure 13 Percent Resolution of  $^4\text{He}$   
in a  $33.8\ \mu$  Si Detector



## 6.0: ALGORITHM DEVELOPMENT

Although several variations of particle identification algorithms have been derived and utilized successfully, few of those existing have a wide range of applicability to many nuclear particles and to a broad range of total energies. Furthermore, their resolution degrades rapidly at low particle energies, which limits their effectiveness for those investigations involving the identification of nuclear particles in the medium to low energy range. Another unfortunate problem with many algorithms is the necessity of adjustable parameters which require modification for each specific application. Therefore, it would be advantageous to produce an algorithm which would have no dependence on adjustable parameters and would exhibit good resolution for a large range of nuclear particles and energies.

Such an algorithm can be derived from the following form of the Bethe-Bloch equation:

$$\frac{dE}{dx} = \frac{-4\pi e^4 Z_i^2 N Z_A \ln \frac{2m_0 V_i^2}{I}}{m_0 V_i^2} \quad 27.$$

Where:

- $e$  = electron charge
- $Z_i$  = effective atomic number of the incident particle
- $N$  = atom density of the absorber
- $Z_A$  = atomic number of the absorber
- $m_0$  = electron rest mass, 511 keV
- $v_i$  = velocity of the incident particle
- $I$  = ionization potential of the absorbing atoms, 177 eV for silicon

The Lorentz contraction term,  $\ln(1-B^2) - B^2$ , has been deleted, since the velocities of the particles of interest are relatively low.

Since  $E_T = m_i v_i^2 / 2$ , substitutions can be made for the incident particle velocity:

$$\ln \frac{2 m_0 v_i^2}{I} = \ln \left[ \frac{E_T \times 12.4}{A_i} \right] \quad 28.$$

$A_i$  represents the mass of the incident particle, while the value 12.4 contains the necessary constants such that  $E_T$  may be expressed in MeV. In a similar manner, the remaining portion of the stopping number expression

may be restated:

$$\frac{4\pi e^4 Z_i^2 N Z_A}{m_0 v_i^2} = 1.66 \times 10^2 \frac{A_i Z_i^2}{E_T} \quad 29.$$

where the numerical constant has the units,  $\text{MeV}^2 \text{cm}^{-1}$ . Equations 28 and 29 may now be combined and rearranged producing an expression which approximates the product of  $A_i Z_i^2$ .

$$A_i Z_i^2 = \frac{6.02 \times 10^1 (dE) (E_T) (dx)^{-1}}{2.52 + \ln E_T - \ln A_i} \quad 30.$$

where  $dx$  is the thickness of the DE detector in microns.

As explained by Green (54), expression 30 is valid only for those instances where  $dE \ll E_T$ , as it assumes that the rate of energy loss of the particle is constant as it traverses the DE detector. However, when the energy of the ion is low or the effective thickness of the DE detector is large, it is necessary to correct for the changing rate of energy loss of the particle as it travels through this detector. One method of approximation uses the following relation for

the average rate of the energy loss:

$$\overline{\frac{dE}{dx}} = \frac{1}{2} \left[ \left( \frac{dE}{dx} \right)_{\text{initial}} + \left( \frac{dE}{dx} \right)_{\text{final}} \right] \quad 31.$$

Where  $(dE/dx)_{\text{initial}}$  refers to the rate of energy loss as the particle enters the DE detector and  $(dE/dx)_{\text{final}}$  refers to the rate as the particle just exits the DE detector. This approximation was used in the final computer application of the following expressions.

In the actual use of this algorithm, we approximate  $A_i$  as  $2Z_i$ . This allows the cube root of each calculation to be used, in order that the particle identification value, PI, will follow  $Z_i$  more linearly. This produces families of curves centered around the atomic number of each element. The following equation illustrates this procedure:

$$PI = K \left( \frac{A_i Z_i^2}{2} \right)^{1/3} \approx K(Z_i) \quad 32.$$

where K is any convenient scaling factor.

Equation 30 is usable in its present form.

When using a 16.6 micron DE detector, its Z resolution is poor beyond oxygen and its mass resolution degrades at  $Z > 4$ , as illustrated in Figure 14. In order to improve the resolution it is necessary to include corrections for the physical deviations that occur in the actual energy loss process of the nuclear particles involved.

At low energies, a correction can be made for the nonparticipation of the inner shell electrons of the atoms of the absorber. For our purpose, only the K-shell correction is necessary. Without this correction, the values of  $A_i Z_i^2$  at lower total energy will be less than that calculated at higher total energies, resulting in a noticeable degradation of the isotopic resolution of the algorithm. This decrease in the value of  $A_i Z_i^2$  is shown in Figure 15.

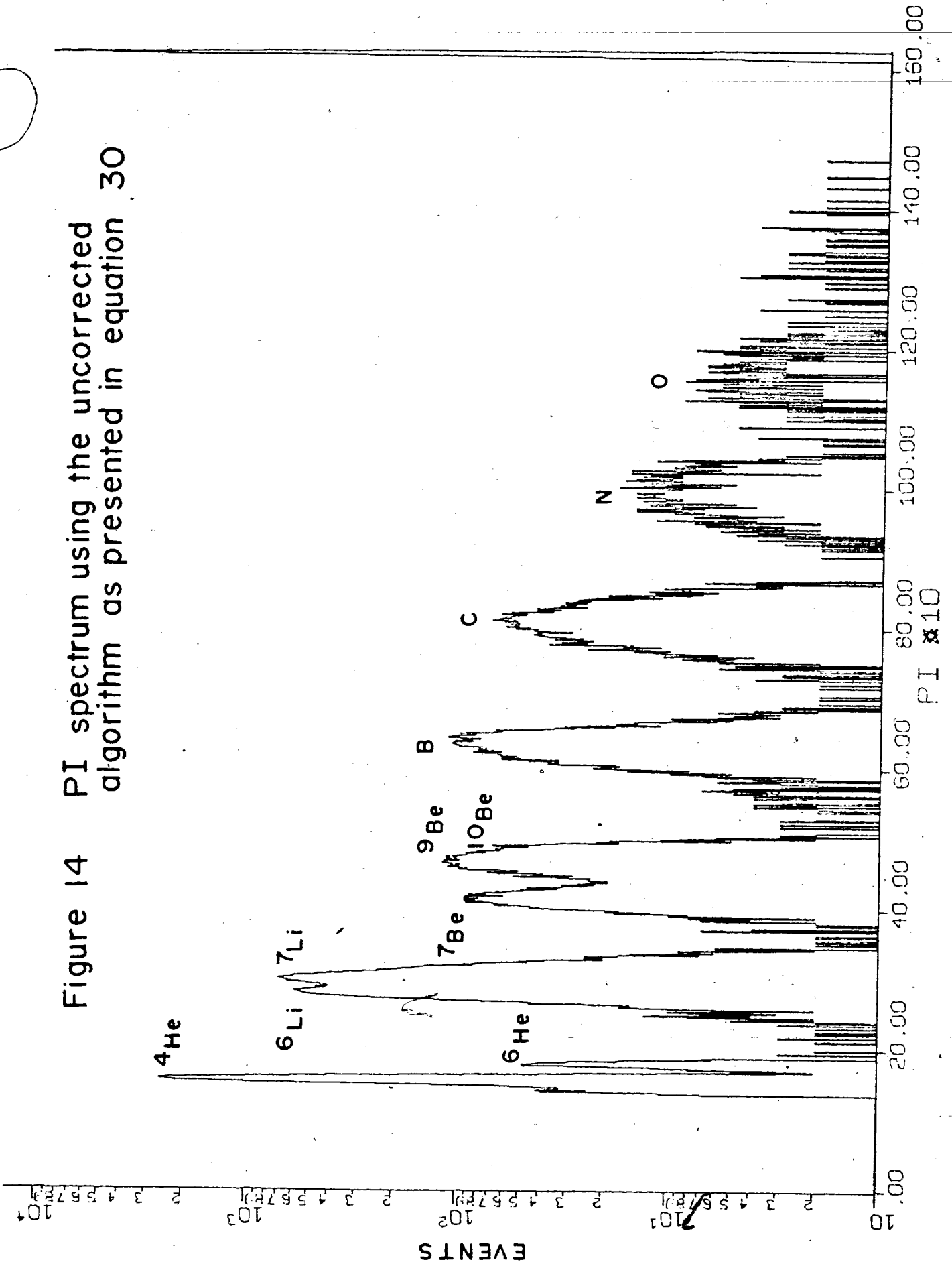
The necessary arguments for approximating this correction term,  $C_k (\theta_k, n_k)$ , have been presented by Walske (8).

$C_k$  is a function of two terms,  $\theta_k$  and  $n_k$ , where:

$\theta_k$  = observed ionization potential of the K-shell  
divided by the ideal ionization potential;

for silicon  $\theta_k = .724$

Figure 14 PI spectrum using the uncorrected algorithm as presented in equation 30



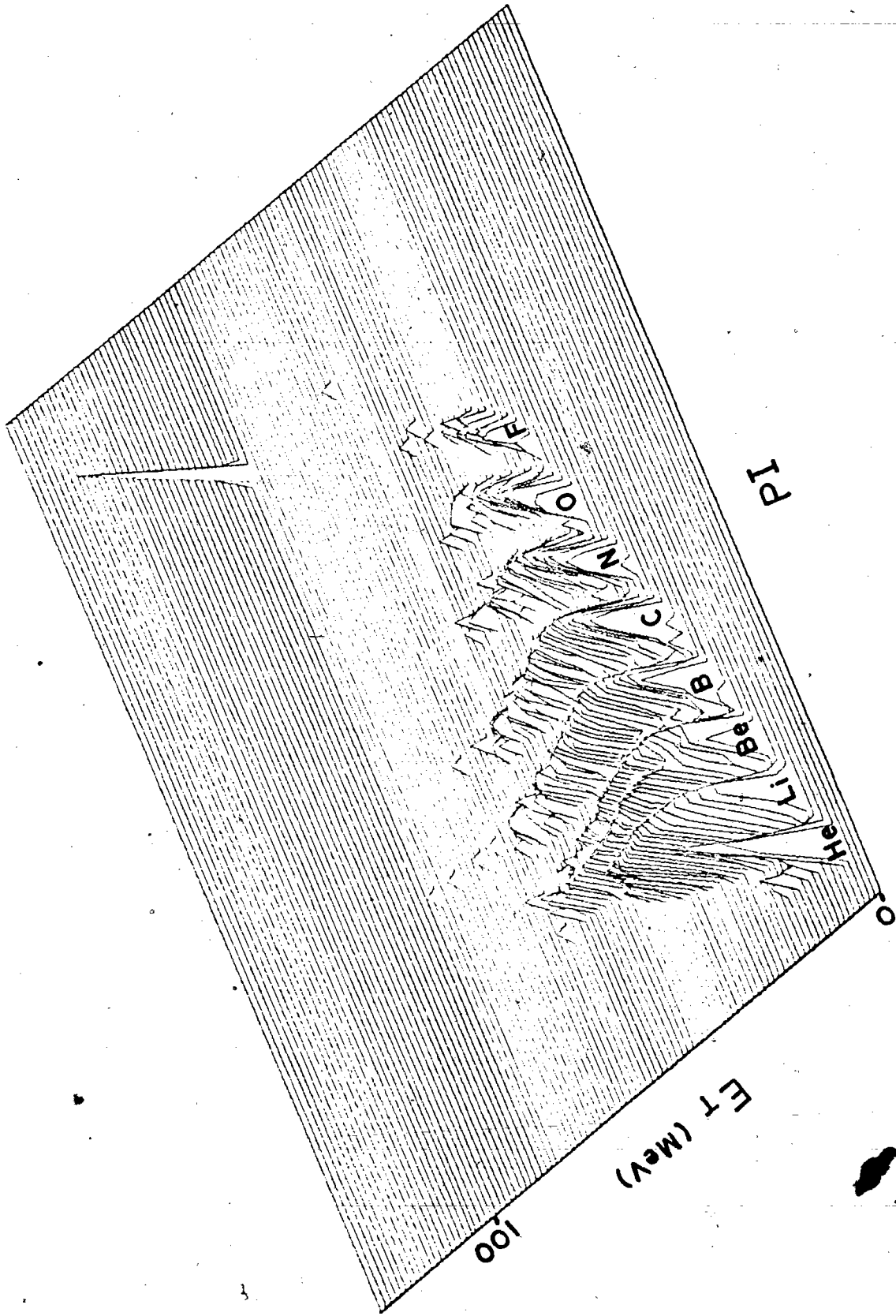


Figure 15. Contour plot of  $E_T$  versus  $PI$  using the uncorrected algorithm as presented in equation 30.

$n_k$  = quantum number related to the K-shell which is given by:

$$n_k = \frac{m_0 V_i^2}{2Z_i^2 R_y} \quad 33.$$

Where  $R_y$  is the Rydberg constant.

By utilizing the earlier expression for the particle velocity,  $V_i = (2E_T/m_i)^{1/2}$ :

$$n_k = \frac{E_T}{A_i Z_i^2 (2.48 \times 10^{-2} \text{ MeV})} \quad 34.$$

Although an exact calculation of  $C_k(\theta_k, n_k)$  is difficult, approximate values can be obtained from Figure 16, which was prepared by Walske. An empirical fit can be calculated for the curve applicable to silicon, for which  $\theta_k = 0.7$ . This approximation takes the following form:

$$C_k = \frac{2.73}{n_k} - \frac{2.34}{n_k^2} + \frac{0.58}{n_k^3} \quad 35.$$

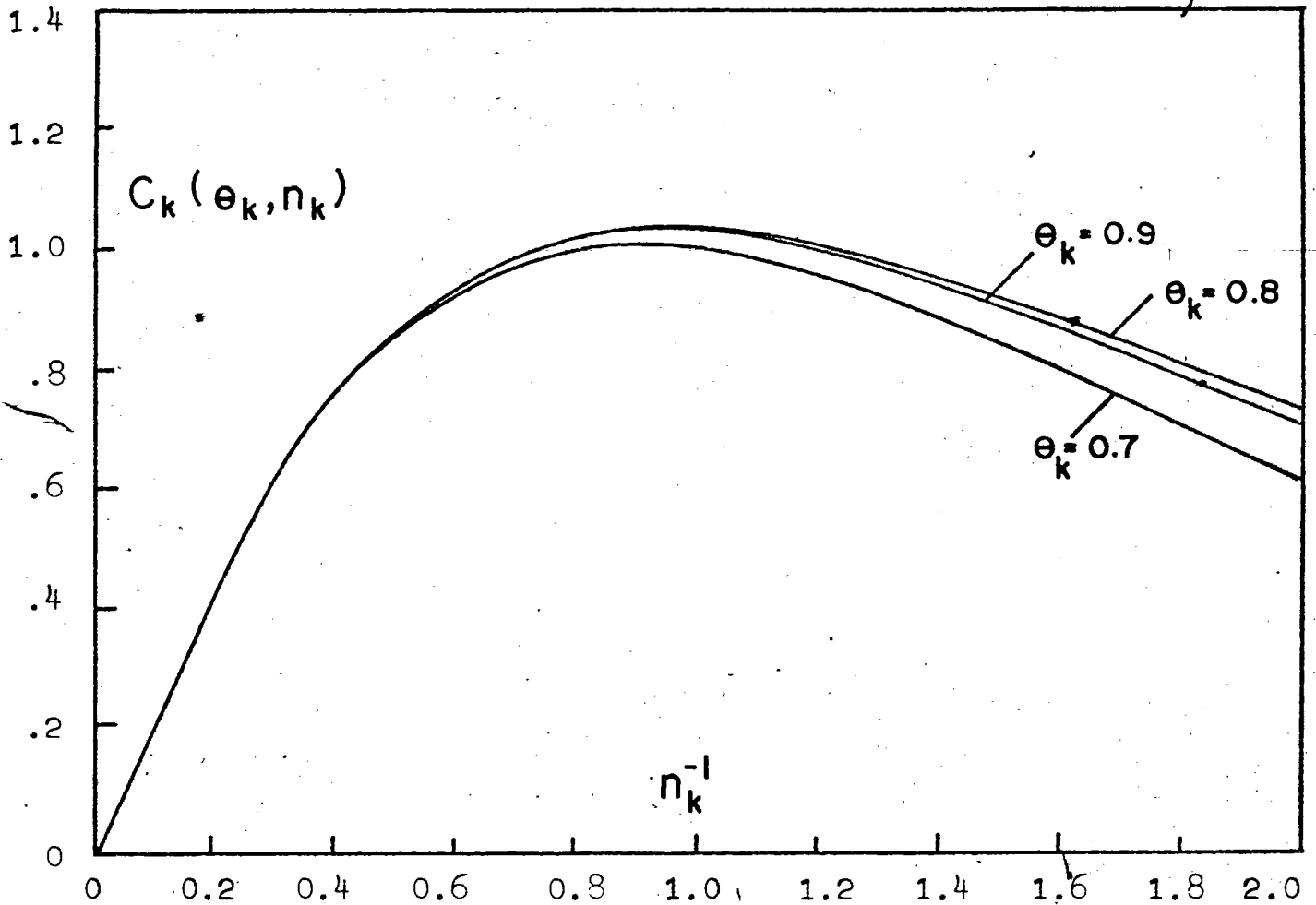


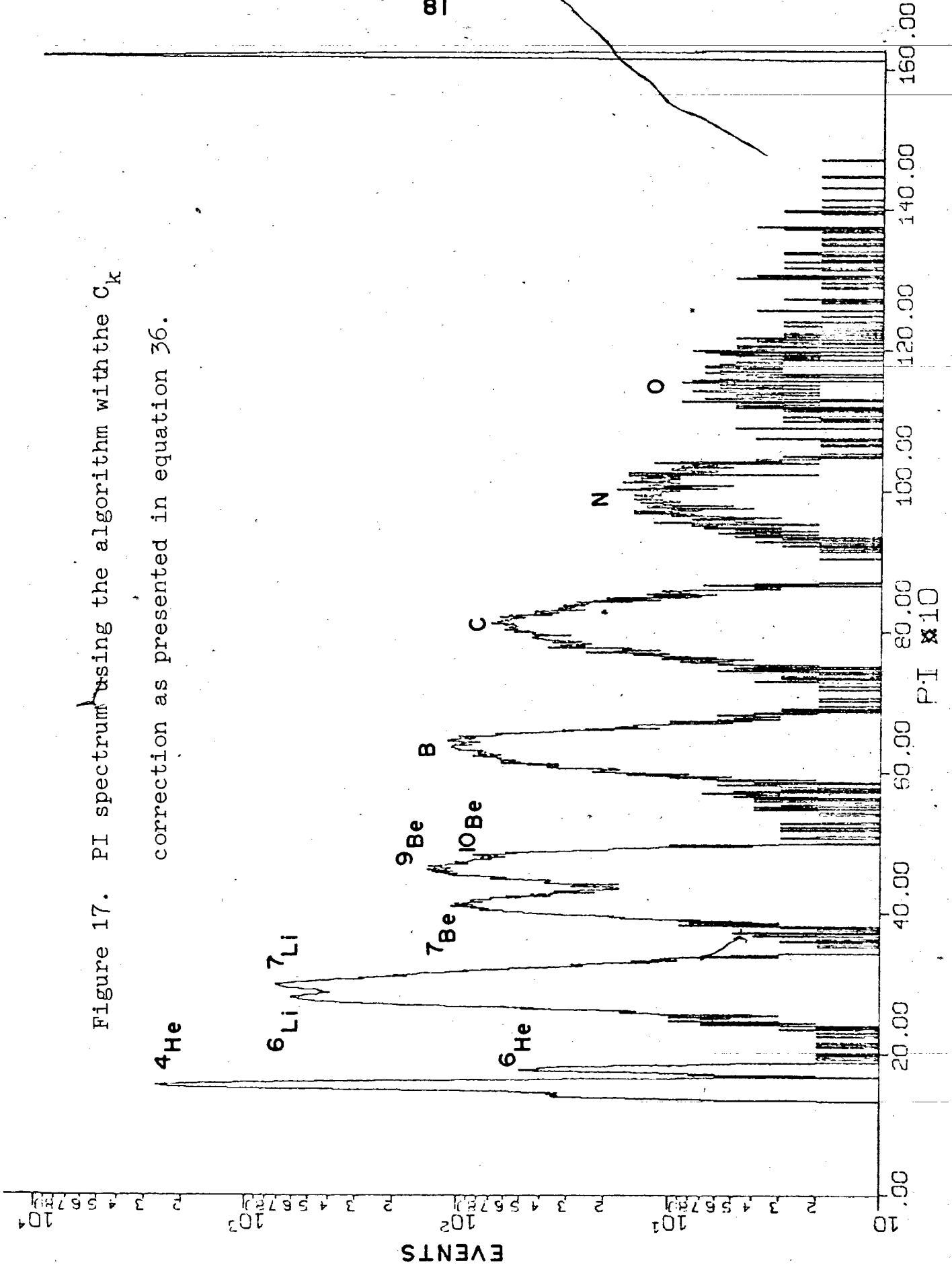
Figure 16. The K-shell stopping number correction is plotted against the reciprocal of the K-shell quantum number.  $\theta_k$  for silicon is 0.724.

Proceeding the calculation of  $n_k$ , the correct value of  $C_k$  ( $\theta_k, n_k$ ) may be calculated using equation 35 and then subtracted from the original stopping number formula, resulting in the corrected value of  $A_i Z_i^2$ :

$$A_i Z_i^2 = \frac{6.02 \times 10^1 (dE)(E_T)(dx)^{-1}}{2.52 + \ln E_T - \ln A_i - \bar{C}_k/14} \quad 36$$

Since the magnitude of this correction will normally increase as the ion slows down, it is necessary to approximate its average value,  $\bar{C}_k$ , in a manner similar to the rate of energy loss. The inclusion of this correction has a marginal effect on the particle resolution of the algorithm, as illustrated by Figure 17. Closer examination of the particle distributions has shown that only low energy protons and alpha particles are effected by this correction, while the particle distributions above  $Z = 2$  remain unchanged. From inspection of Figure 18, it is evident that for those particles above boron the calculated values of  $A_i Z_i^2$  decreases with decreasing total energy. Two different effects could contribute to this deviation. First, these particular particles are approaching velocities which are equivalent to the velocity of the L-shell electrons in the silicon of the

Figure 17. PI spectrum using the algorithm with the  $C_k$  correction as presented in equation 36.



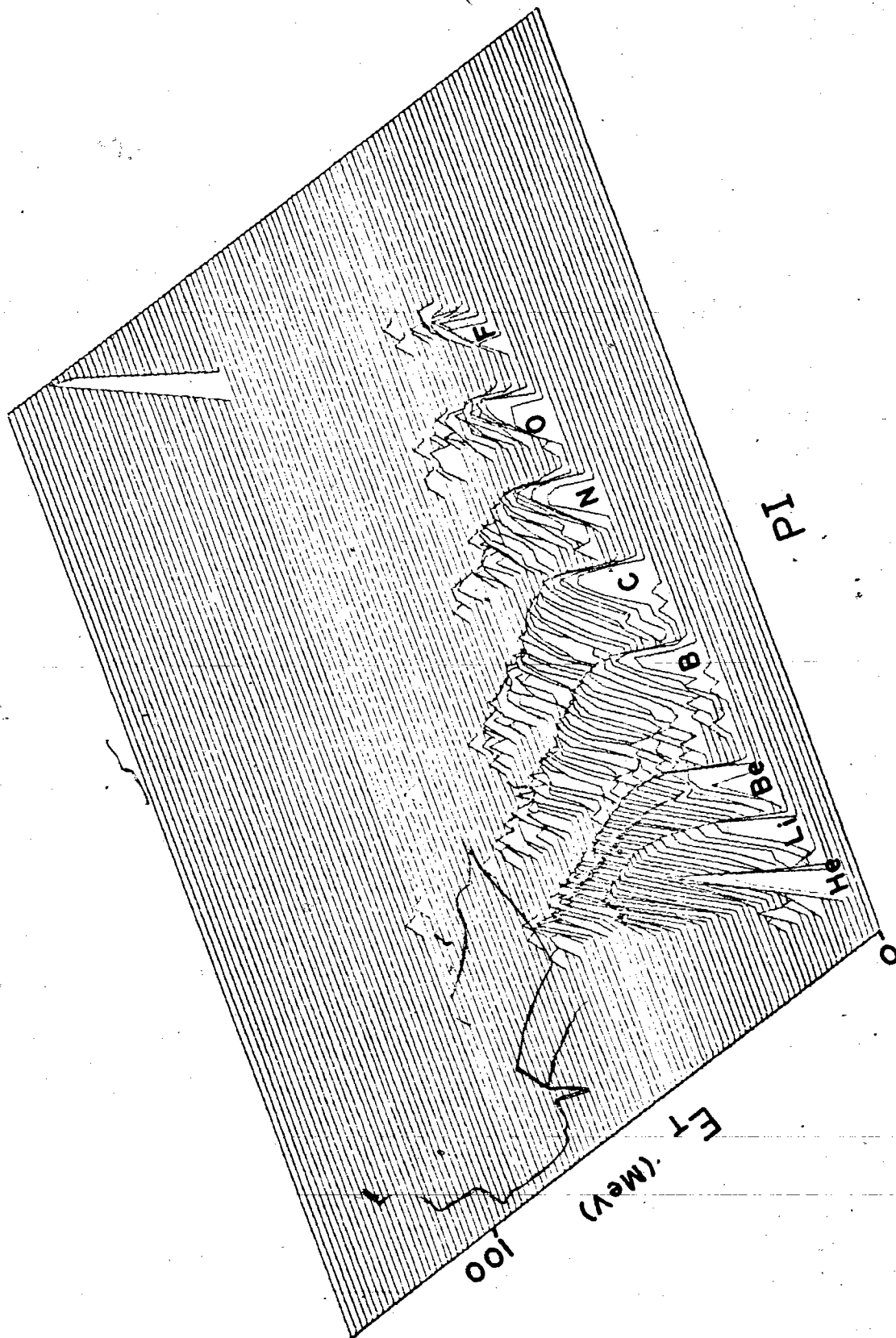


Figure 18. Contour plot of  $E_T$  versus  $PI$  using the algorithm with the  $C_k$  correction as presented in equation 36.

DE detector. This would suggest that a  $C_L$  correction, analogous to the  $C_k$  correction, be added. However, the magnitude of this correction, as described by Walske (9), is far too small to cause any change, as its magnitude is less than that of the  $C_k$  correction.

A more probable explanation is the occurrence of charge pick-up by the lower energy nuclear particles before or during their passage through the DE detector. This is reasonable because the Bethe-Bloch equation predicts the effective charge of the particle involved. Therefore, if a particle fails to remain completely stripped during its passage through the DE detector, one would expect a lower value of  $A_i Z_i^2$ , as observed.

Booth and Grant (46) have studied the charge pick-up of heavy ions. Using their own measurements as well as data from Porat (47),(48), Phillips (49), Teplova et al (50), Moak (51), and Northcliffe (52); they have succeeded in preparing a universal curve which relates the variation of effective charge to the particles' s velocity and atomic number, independent of the stopping material. This curve, as presented in Figure 19, only covers those values of  $\gamma_{\text{eff}}^2 < 0.80$ , where  $\gamma_{\text{eff}} Z_0 = Z_i$ . In order to incorporate this

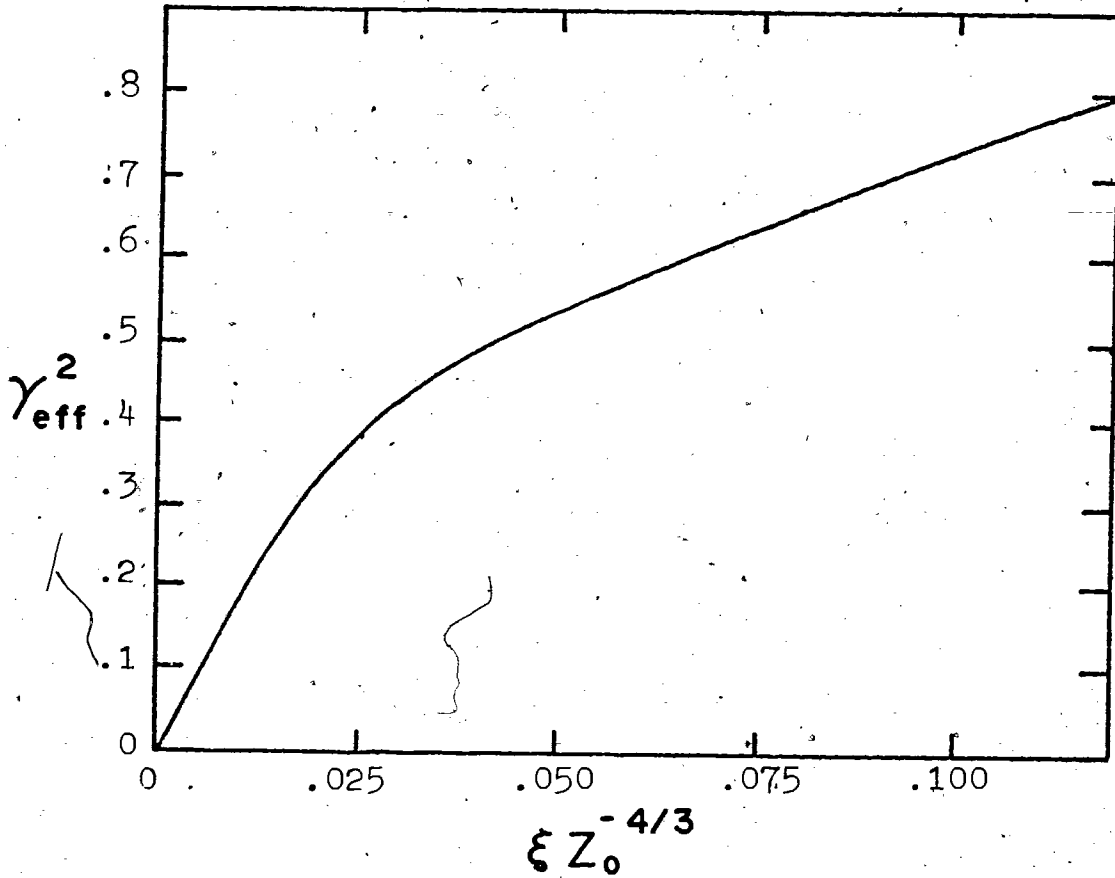


Figure 19. The effective charge of heavy ions as a function of the particle's charge and energy.

correction into the PI expression, it is necessary to calculate an expression which represents this curve as a function of  $\xi Z_0^{-4/3}$ ; where  $\xi$  is the energy of the particle in MeV/amu. Furthermore, this expression must be extended to approach  $\gamma_{\text{eff}}^2 = 1.0$  asymptotically, in order that the higher velocity ions receive adequate correction. This is easily accomplished and takes the following form:

$$\gamma_{\text{eff}}^2 = 20.7(\xi Z_0^{-4/3}) - 236.0(\xi Z_0^{-4/3})^2 + 986.9(\xi Z_0^{-4/3})^3 \quad \text{for } \xi Z_0^{-4/3} \leq 0.10 \quad 37a$$

$$\gamma_{\text{eff}}^2 = 1.0 - \exp \left[ \frac{-\xi Z_0^{-4/3}}{0.08} \right] \quad \text{for } \xi Z_0^{-4/3} > 0.10 \quad 37b$$

Relation 37a is valid for  $\xi Z_0^{-4/3} < 0.10$ . Above this value the magnitude of  $\gamma_{\text{eff}}^2$  increases too rapidly and an alternative relation must be used. Expression 37b is used when  $\xi Z_0^{-4/3} > 0.10$ . This expression approaches  $\gamma_{\text{eff}}^2 = 1.0$  asymptotically and corrects the value of  $Z_i$  for these higher velocity ions. The parameter  $\xi Z_0^{-4/3}$  is given by:

$$\xi Z_0^{-4/3} = \frac{E_T(Z_0)^{-4/3}}{\exp\{.33 \ln(4A_i Z_i^2)\}} \quad 38.$$

Where  $Z_0$  is the stripped charge of the nuclear particle. The average value of the charge correction,  $\bar{\gamma}_{eff}^2$ , is used in the actual calculation. This yields a better approximation to the correction as previously described. The corrected value of  $A_i Z_i^2$  may be obtained using the following operation.

$$A_i Z_0^2 = \frac{A_i Z_i^2}{\bar{\gamma}_{eff}^2} \quad 39.$$

By including this charge pick-up correction, much straighter particle distributions are obtained as shown in Figure 20. Furthermore, the isotopic resolution is improved as several peak-to-valley ratios are increased, as illustrated in Figure 21. Some curve is still observable in the higher mass distributions. This is a result of the function chosen to approximate  $\bar{\gamma}_{eff}^2$ . More experimental data, concerning the charge pick-up of heavy ions, would be necessary to improve this function.

The final form of the algorithm is given by:

$$A_i Z_0^2 = \frac{6.02 \times 10^1 (dE)(E_T)(dx)^{-1} (\bar{\gamma}_{eff})^2}{2.52 + \ln E_T - \ln A_i - \bar{C}_k/14} \quad 40.$$

Figure 20. Contour plot of  $E_T$  verses PI using the algorithm with both the  $C_k$  and the charge pick-up corrections as presented in equation 40.

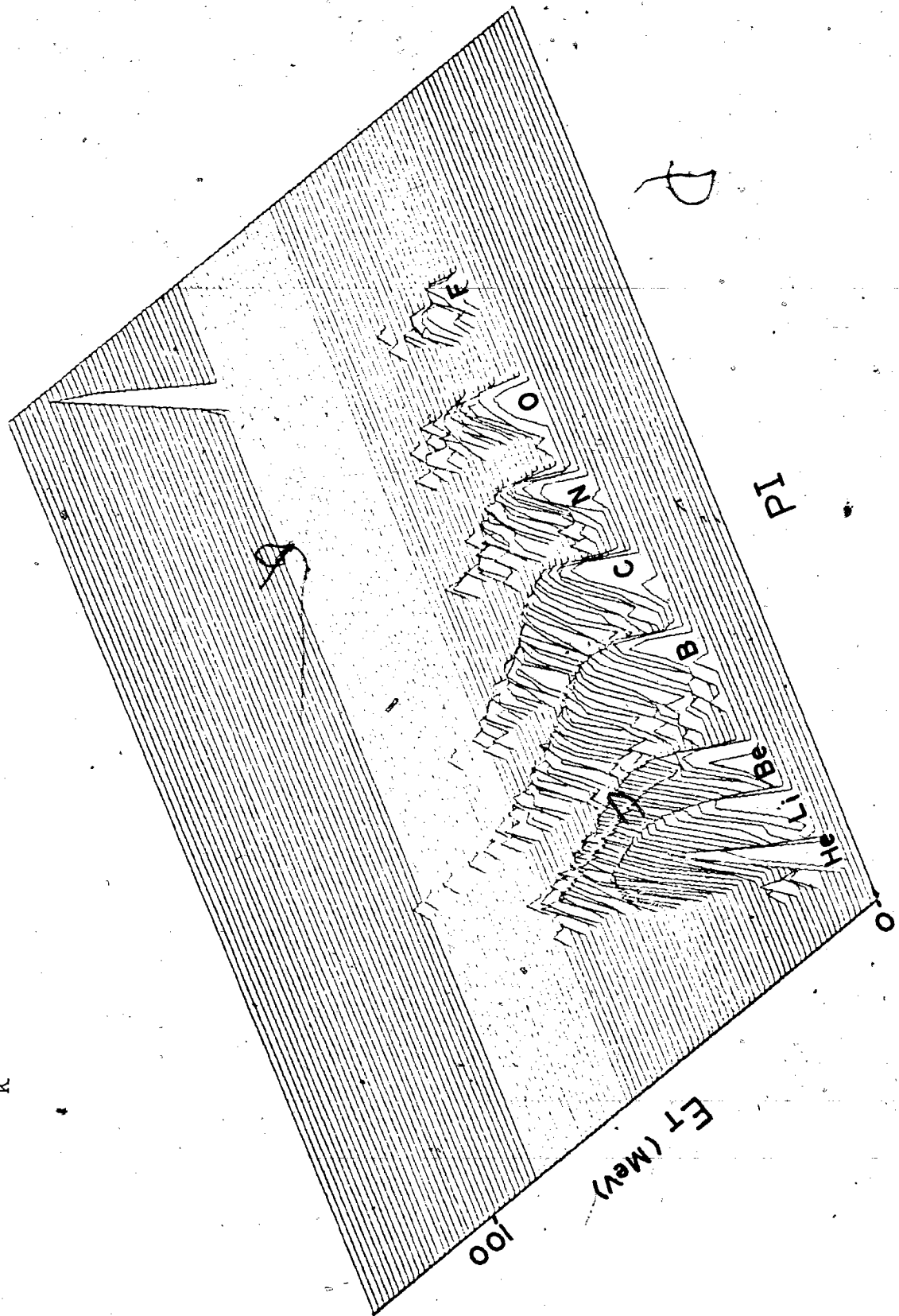
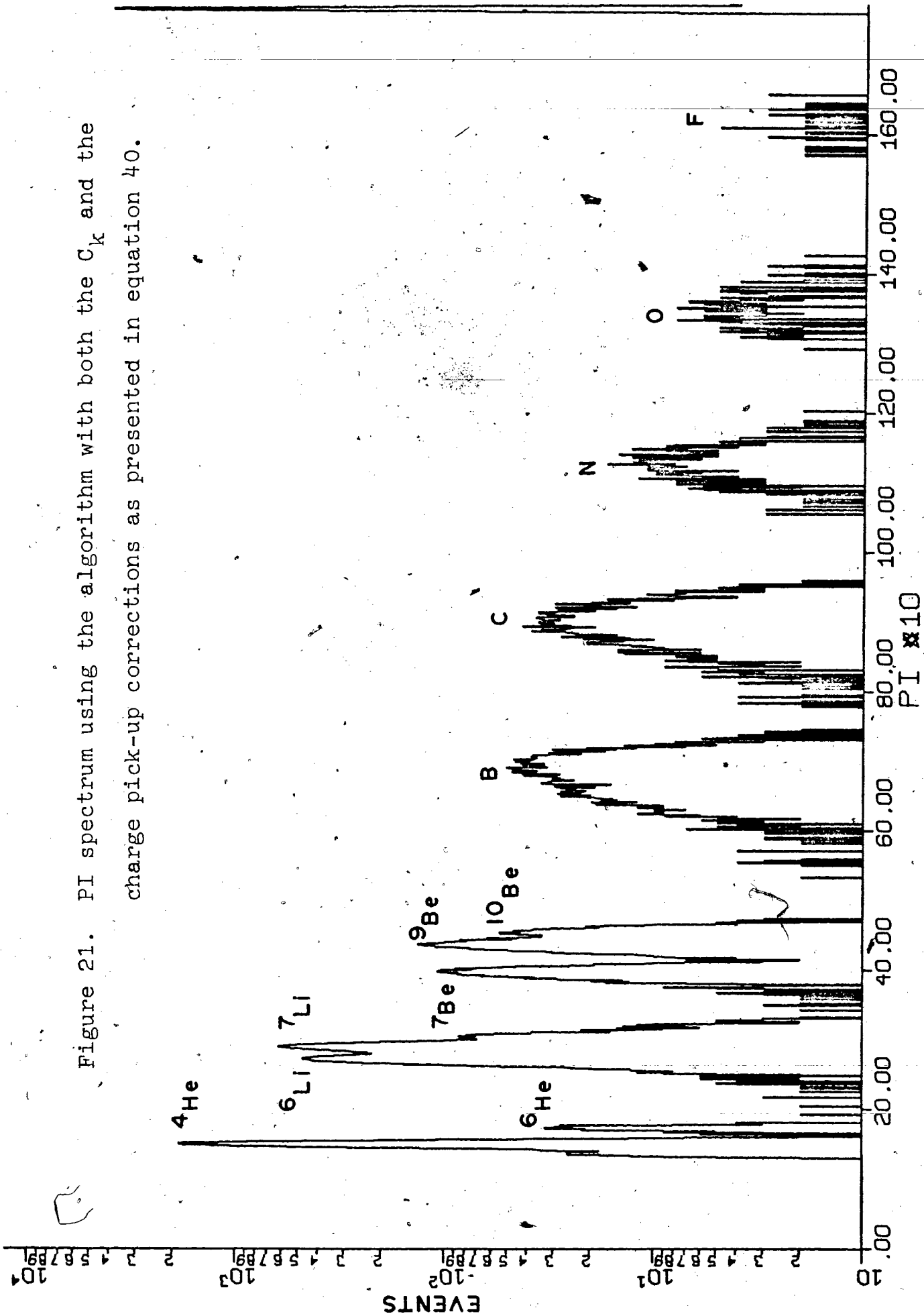


Figure 21. PI spectrum using the algorithm with both the  $C_k$  and the charge pick-up corrections as presented in equation 40.



with the particle identification value, PI, given by:

$$PI = K \left[ \frac{A_i Z_o^2}{2} \right]^{1/3} \quad 41.$$

The  $C_k$  correction is included although its effect is marginal in the case studied here, as previously explained.

The final form, as expressed by equation 40 contains no unknown adjustable parameters, nor is it restricted to any one telescopic configuration. All of the parameters are either known, measured, or calculated from the measured values of  $dE$  and  $E_T$ . In the use of this expression, a value of  $Z_i$  is initially assumed, to allow the calculation of appropriate values of  $\bar{C}_k$  and  $\bar{\gamma}_{eff}^2$ . Following the use of expression 40, the resultant value of  $Z_o$  is passed back for a new approximation of the correction terms. This is continued in a bootstrap fashion, until a constant value of  $Z_o$  is obtained.

It is mandatory that the method one chooses to analyze the data does not degrade the inherent resolution of the detector telescope used in the experiment. One can graph the raw  $DE-E_T$  data with the

calculated PI values. This was done in the lithium region and is illustrated in Figure 22. The PI distribution is integrated over all values of  $E_T$ , 10-50 MeV, while the dE distribution is taken from a narrow window of  $E_T$  at 15.0-15.5 MeV. By inspection, it is apparent that no loss of resolution results from the use of this algorithm.

It is also advantageous for the algorithm to calculate constant values of PI for given isotopes, regardless of the DE detector thickness. Table III lists the values of  $A_i Z_o^2$  calculated from data taken by telescopes with varying configurations. Although the values of  $A_i Z_o^2$  deviate as one increases in mass, the values obtained from two different systems are relatively constant.

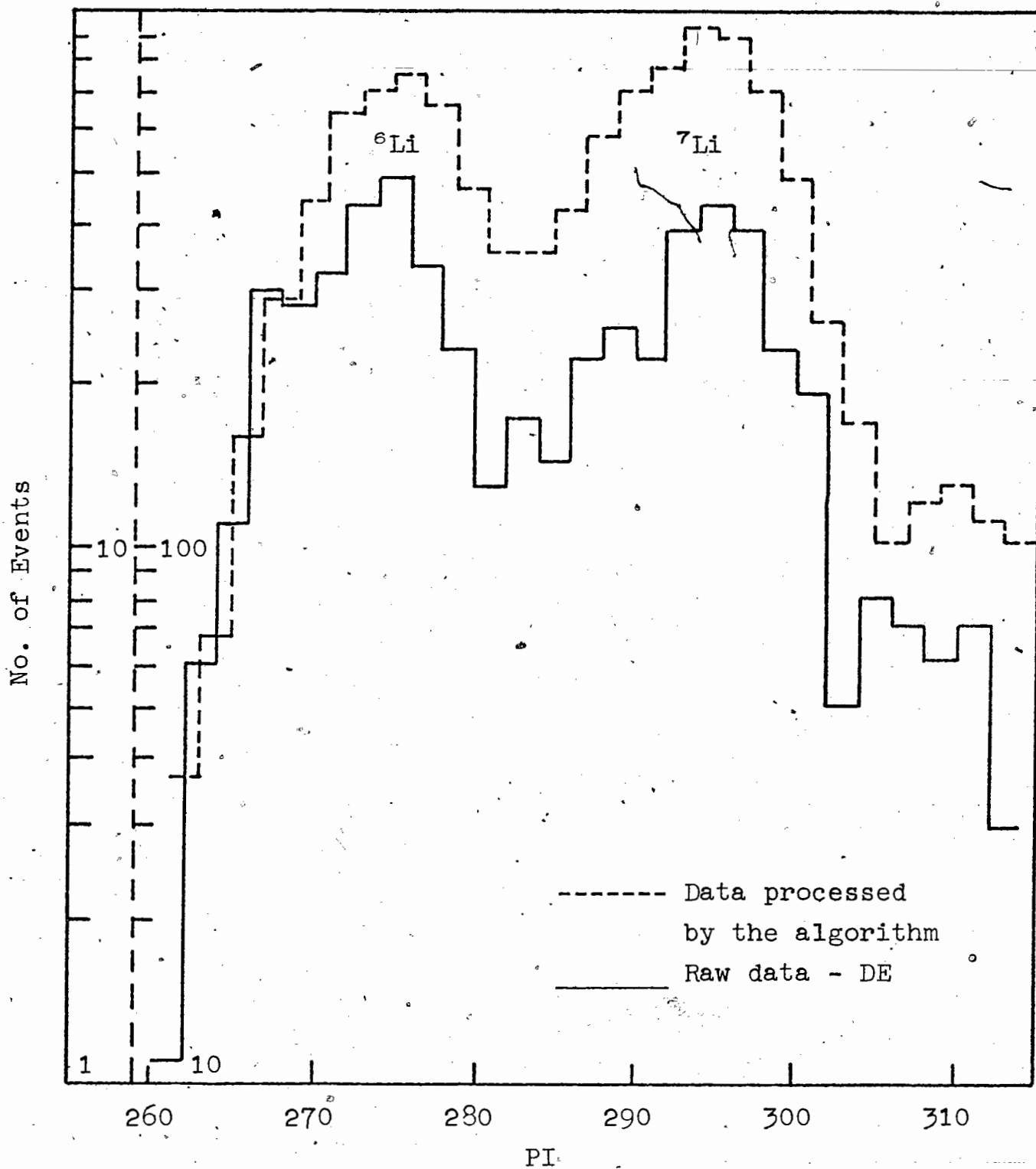


Figure 22. Raw DE data and related PI values for the Lithium region.

TABLE III: Values of  $A_i Z_O^2$  calculated  
from the final PI algorithm

DE (microns)	$^4\text{He}$	$^6\text{Li}$	$^7\text{Be}$	$^{10}\text{B}$	$^{12}\text{C}$
12.9	15	52	113	256	440
16.6	15	53	115	260	443
Theoretical	16	54	112	250	432

## CONCLUSION

From the straggling measurements presented, one observes that as the incident ion energy increases, the FWHM of the energy loss distribution in the DE detector decreases. This trend is the result of both a decrease in the statistical and the non-statistical fluctuations. As an ion's energy increases it will lose less energy per interaction, resulting in a narrower energy loss distribution. Similarly, the higher energy particles are less likely to capture electrons. If this does occur, the frequency of the charge changing process will be sufficiently high to keep charge broadening to a minimum.

From the trends of the straggling widths, it would be expected that the energy resolution of the DE detectors would be highest for those particles with the largest kinetic energy. However, due to the fact that the straggling width levels out at higher energies as a result of the inherent noise of the system, the optimum energy resolution is reached at particle energies coinciding with energy depositions of 20-40 %.

However, satisfactory energy resolution can be

obtained at higher or lower energies. For example, the poorest resolution measured in both the proton and alpha particle case is sufficient to separate them from neighboring nuclides of the same atomic number as is evident from Figure 6. However, as the value of  $MZ^2$  increases, the available energy resolution becomes more critical. In these circumstances, extensive straggling measurements would allow the experimentalist to choose a DE detector which would offer the best resolution for the particles and energies of interest.

Aside from the choice of the telescopic configuration, it has been shown that the isotopic resolution of the DE-E technique can be improved by the development of particle identifying algorithms which are based on theoretical considerations rather than empirical relations. Algorithms of this type offer not only improved resolution, but are valid over larger ranges of particles and energies. We have demonstrated that the  $C_k$  correction has a marginal effect on the particle resolution of the energy range studied, whereas the charge correction is very important in extending the algorithm to the lower particle energies used in this investigation.

The particle spectra presented in the previous chapter only indicate the particle resolving power of the developed algorithm. However the data tested is representative of the particles and energies observable in a typical fragment experiment. The measured values of the percent resolution and the satisfactory particle separation obtained with the new algorithm can now be applied to the fragment study.

## APPENDIX A:

## 1.0: CORRELATION COEFFICIENT.

In order to determine if the variations in the straggling widths are reproducible and statistically significant, one may test the degree of linear correlation between two distributions measured under identical conditions. For two such distributions, a measurement of the linear correlation coefficient ( $r$ ) will give the degree of the linear relationship (53).

The linear correlation between any pair of widths  $X$  and  $Y$  measured at a given particle energy or velocity, can be expressed as follows:

$$Y = a + bX \quad 1.$$

where the slope ( $b$ ) is given by:

$$b = \frac{N \sum_{i=1}^n X_i Y_i - \sum_{i=1}^n X_i \sum_{i=1}^n Y_i}{N \sum_{i=1}^n X_i^2 - \left( \sum_{i=1}^n X_i \right)^2} \quad 2.$$

where  $N$  is the number of sets of measurements being compared.

If no correlation exists between the set of widths, any tendency for Y to increase or decrease with a rise in X will not be evident.

We may also look at X as a function of Y:

$$X = a' + b' Y \quad 3.$$

with  $b'$  being similar to  $b$  as follows:

$$b' = \frac{N \sum_1^n X_i Y_i - \sum_1^n X_i \sum_1^n Y_i}{N \sum_1^n Y_i^2 - (\sum_1^n Y_i)^2} \quad 4.$$

If a complete correlation exists between X and Y, then a relationship between the coefficients  $a, b$  and  $a', b'$  must also exist:

$$Y = -a'/(b') + (1/b') X \quad 5.$$

$$= a + bx$$

which implies that  $a = -a'/b'$  and  $bb' = 1$ . In the case of negligible or no correlation, the values of  $b$  and  $b'$  are zero, as the variation of Y is not proportional to the variation of X.

Therefore, one may utilize the experimental linear correlation coefficient  $r$  which equals the product of  $b$  and  $b'$  as a measure of the degree of linear correlation.

$$\text{With: } r = \frac{N \sum_{i=1}^n X_i Y_i - \sum_{i=1}^n X_i \sum_{i=1}^n Y_i}{\left\{ \left[ N \sum_{i=1}^n X_i^2 - \left( \sum_{i=1}^n X_i \right)^2 \right] \left[ N \sum_{i=1}^n Y_i^2 - \left( \sum_{i=1}^n Y_i \right)^2 \right] \right\}^{1/2}} \quad 6.$$

This relation will give values ranging from 0, when no correlation exists, to 1, when there is complete correlation.

## APPENDIX B

## 1.0: STRAGGLING THEORY OF TSCHALAR

Tschalar (20,21,22) has investigated the problem of calculating  $f(T,x)$  in thick absorbers, where  $f(T,x)$  represents the distribution of residual energies,  $T$ , after traversing a thickness,  $x$ , of an absorbing medium. These distributions can be described by their mean energy,  $T_{av}$ , their variance,  $\sigma_2$ , and their reduced third central moment,  $\gamma_3$ , where:

$$T_{av}(x) = \int_0^{\infty} f(T,x) T dt$$

$$\sigma_2(x) = \int_0^{\infty} f(T,x) (T - T_{av})^2 dt$$

$$\gamma_m(x) = \sigma_m (\sigma_2)^{-m/2}$$

for integers  $n$  and  $m$ .

The standard deviation is given by  $\sigma = \sigma_2^{1/2}$  and is a measure of the width of the distribution. The skewness is given by  $\gamma_3$  where  $\gamma_3 = 0$  for symmetric distributions.

The calculation of  $f(T,x)$  is based on the collision probability  $P(Q,T)dQdx$ . Here,  $T$  is the energy of the ion before the collision and  $Q$  is the energy transferred.

The fact that the energy loss in each collision is a stochastic variable produces a spreading of the energies of the monoenergetic incident particles as they pass through the medium. For small values of  $x$  the energy distribution,  $f(T,x)$ , is governed by the  $Q$ -dependence of  $P(Q,T)$  since  $T$  remains relatively constant over the width of the distribution. This region is referred to as the "stochastic region".

However, with an increase of the width of  $f(T,x)$  the energy  $T$ , after traversing a given path length  $x$  can no longer be considered constant. The  $T$ -dependence of  $P(Q,T)$  now influences the shape of  $f(T,x)$  significantly. This region is defined as the "bulk region".

The collision spectrum,  $P(Q,T)$ , chosen for the following equations is based on classical collisions with free absorber electrons. The collision

probability is given by:

$$P(Q, T) = \frac{1}{2}(k/T)Q^{-2}, \text{ if } Q_{\min} \leq Q \leq Q_{\max}$$

$$= 0, \text{ otherwise.}$$

$$Q_{\max} = 4u(1 + u)^{-2}T = \epsilon T$$

$$Q_{\min} = I^2/(\epsilon T)$$

$$k = 2\pi e^4 Z_i^2 Z_A N/u$$

$$\epsilon = 4(m_0/M_i)\{1 + (m_0/M_i)\}^{-2}$$

where  $M_i$  is the mass of the incident particle. The term  $\mu$  represents the ratio of the electron mass to the particle mass and is defined as:

$$\mu = \epsilon T/I$$

The variance  $\sigma_2$  has been solved numerically and is given by

$$\sigma_2(T_{av}) = K_1^2(T_{av}) \int_{T_0}^{T_{ov}} \frac{K_2}{K_1^3} dT$$

Where  $K_1 = P(Q,T)QdQ$  and  $K_2$  is the variance of  $P(Q,T)$ .

The application of this theory begins with the generation of the ~~moments~~ moments of  $f(T,x)$ , to which mathematical distributions are then fitted. Tschalar has calculated these moments for a number of ions including protons and alpha particles, with energy losses ranging from zero to 90%. Graphs were generated of  $\sigma_2$ , multiplied by  $(\log u_0) \times (\epsilon_p/\epsilon)(T_0 - T_{av})^{-1}$ , verses  $T_{av}/T_0$ .

The experimenter can extract theoretical straggling widths from the available graphs as follows. First, one calculates the reduced energy  $\mu$  using equation 5. This result, combined with the value of  $T_{av}/T_0$ , allows the term containing  $\sigma_2$  to be chosen. Since all of the parameters in this term are known,  $\sigma_2$  can be easily calculated. The straggling width is finally given by the statistical expression for the FWHM.

$$FWHM = \sigma (2.35)$$

The addition of the charge pick-up correction would require an alteration of the collision spectrum

P(Q,T). The general result would be a decrease in the value of P(Q,T) with a decrease in particle energy.

The atomic binding correction would also require a modification of P(Q,T), since the limits of the energy transferred in a collision are dependent on the average excitation potential. This correction would also alter the value of the reduced energy depending on the residual energy of the particle. With higher energy losses this effect would decrease  $\mu$  which would increase the value of  $\sigma_2$ .

## REFERENCES

- 1) Bichsel H., Nucl. Inst. Meth. 78, (1970) 277
- 2) Uehling E., Ann. Rev. of Nucl. Sci. 4, (1954) 315
- 3) Bohr N., Phil. Mag. 25, (1913) 10
- 4) Bohr N., Phil. Mag. 30, (1915) 581
- 5) Bethe N., Ann. Physik 5, (1930) 325
- 6) Paul J., Nucl. Inst. Meth. 94, (1971) 275
- 7) Whaling W., Nuclear Spectroscopy Vol. A, (1960) 3-16, Ajzenberg
- 8) Walske M., Phys. Rev. 88, (1952) 1283
- 9) Walske M., Phys. Rev. 101, (1956) 940
- 10) Sternheimer R., Phys. Rev. 145, (1966) 147
- 11) Lindhard J., Scharff M., Schiott H., Mat. Fys. M. Dan. Vid. Selsk. 33, (1963)
- 12) Northcliffe, L.C., Nucl. Data Tables A-7, (1970) 233-465
- 13) Armstrong T., Chandler K., Nucl. Inst. Meth. 113, (1973) 313
- 14) Steward P., Ph.D. Thesis, (1968), Berkely
- 15) Bohr N., Kgl. Danske Vid. Selsk. Mat. Fys. Medd. 18, (1948) 8
- 16) Landau L., J. Phys. U.S.S.R. 8, (1944) 201
- 17) Symon K., Ph.D. Thesis, (1948) Harvard
- 18) Vavilov P., Sov. Phys. JEPT 5, (1957) 749
- 19) Seltzer S., Berger M., Natl. Acad. Sci., Natl. Res. Coun. Pub. 1133, (1964) 187
- 20) Tschalar C., Nucl. Inst. Meth. 61, (1968) 141
- 21) Tschalar C., Nucl. Inst. Meth. 64, (1968) 237

- 22) Tschalar C., Maccabee H., Phys. Rev. B 1, (1970) 2863
- 23) Payne M., Phys. Rev. 185, (1969) 611
- 24) Maccabee H., Ph.D. Thesis, (1966), Berkely
- 25) Maccabee H., Raju M., and Tobias C., Phys. Rev. 165, (1968) 469
- 26) Bertolini G., Coche A., "Semiconductor Detectors", (1968) John Wiley and Sons, Inc, New York
- 27) Poenaru D.N., Vilcov N., "Measurement of Nuclear Radiation with Semiconductor Detectors", (1969) Chemical Publishing Co., Inc., New York
- 28) Ortec, " Silicon Surface Barrier Radiation Detectors", Pub # 2371-05k-0975, (1975)
- 29) Wang L., Zatzick M., Ziembra S., IEEE TRANS. Nucl. Sci. NS11 NO. 1, (1964) 314
- 30) Goulding F.S., Harvey B.G., Ann. Rev. Nuc. Sci. 25, (1975) 167-240
- 31) Barrette J., Braun-Munzinger P., Gelbke C.E., Nuc. Inst. Meth. 126, (1975) 181-187
- 32) Butler G.W., Poskanzer A.M., Landis D.A., Nuc. Inst. Meth. 89, (19) 189-198
- 33) Goulding F., Landis D., Cerny J., Pehl R., Nuc. Inst. Meth. 31, (1964) 1
- 34) Goulding F., Landis D., Cerny J., Pehl R., IEEE Trans. Nucl. Sci. NS-13 #3, (1966) 514
- 35) Schneider W., Nuc. Inst. Meth. 123, (1975) 93-98
- 36) Bowman J., Poskanzer A., Korteling R., Butler G., Phys. Rev. C. 9, (1974) 836
- 37) Korteling R., Toren R., Hyde E., Phys. Rev. C. 7, (1973) 1611
- 38) Chulick E.T., Natowitz J.B., Schnatterly C., Nuc. Inst. Meth. 109, (1973) 171-175

- 39) Lindhard J., Nielson V., Phys. Lett. 2, (1962) 209
- 40) Maples Jr. C., Cerny J., unpublished
- 41) Steward P.G., Lawrence Radiation Laboratory Report No. UCRL-18127, 1968
- 42) Avdeichikov V., Nucl. Inst. Meth. 118, (1974) 247
- 43) Armitage B., Trehan P., Nucl. Inst. Meth. 134, (1976) 359
- 44) Schmidt K., Wohlfarth H., Clerc H., Lang W., Schrader H., Pferdekamper K., Nucl. Inst. Meth. 134, (1976) 157
- 45) Kolota J., Amos T., Phys. Rev. 176, (1961) 484
- 46) Booth W., Grant I., Nucl. Phys. 63, (1965) 481-495
- 47) Porat D.E., Ramavataram K., Proc. Phys. Soc. 77, (1961) 97
- 48) Porat D.E., Ramavataram K., Proc. Phys. Soc. 78, (1961) 1135
- 49) Phillips W.R., Read F.H., Proc. Phys. Soc. 81, (1963) 1
- 50) Teplova Y.A., Nikolaev V.S., Dmitriev I.S., Fateeva L.N. JETP 15, (1962) 31
- 51) Moak C.D., Brown M.D., Phys. Rev. Lett. 11, (1963) 284
- 52) Northcliffe L.C., Ann. Rev. Nucl. Sci. 13, (1963) 67
- 53) Mendenhall W., Introduction to Probability and Statistics, Duxbury Press, London, (1971)
- 54) Green R., private communication